
BaCaDI: Bayesian Causal Discovery with Unknown Interventions

Alexander Hägele^{1*}, Jonas Rothfuss¹, Lars Lorch¹, Vignesh Ram Somnath^{1,3},
Bernhard Schölkopf^{2,1}, Andreas Krause¹

¹Department of Computer Science, ETH Zürich, Switzerland

²Max Planck Institute for Intelligent Systems, Tübingen, Germany

³IBM Research Zürich, Switzerland

Abstract

Learning causal structures from observation and experimentation is a central task in many domains. For example, in biology, recent advances allow us to obtain single-cell expression data under *multiple interventions* such as drugs or gene knockouts. However, a key challenge is that often the *targets of the interventions are uncertain or unknown*. Thus, standard causal discovery methods can no longer be used. To fill this gap, we propose a Bayesian framework (BaCaDI) for discovering the causal structure that underlies data generated under various unknown experimental/interventional conditions. BaCaDI is fully *differentiable* and operates in the continuous space of latent probabilistic representations of both causal structures and interventions. This enables us to approximate complex posteriors via gradient-based variational inference and to reason about the epistemic uncertainty in the predicted structure. In experiments on synthetic causal discovery tasks and simulated gene-expression data, BaCaDI outperforms related methods in identifying causal structures and intervention targets. Finally, we demonstrate that, thanks to its rigorous Bayesian approach, our method provides well-calibrated uncertainty estimates.

1 Introduction

Identifying causal dependencies by empirical observation and experimentation is a problem of fundamental scientific interest. If we understand the causal mechanisms that govern a system of interest, we can predict its behavior when parts of system are actively manipulated from outside. For instance, if we understand the causal structure of a gene regulatory network, we can predict the effect of drugs or gene knockouts more reliably [42]. While identifying the true causal structure from observational data is impossible in many cases [46, 47], intervening on some variables in the system and observing the outcome can provide valuable information helping with identification.

In some settings, we can collect a range of datasets from the same causal system under multiple different interventions. For instance, recent advances in biology allow us to obtain single-cell gene expression data under interventions such as different drug candidates or gene knockouts [58, 41]. Causal discovery methods that can work with interventional data typically assume knowledge of the targets, i.e., which variables have been intervened upon, or the statistical effect of the interventions [23, 60, 62]. However, this limits their applicability because the intervention targets and effect are often *uncertain or unknown* in practice, for instance, due to unknown off-target effects upon drug administration. An additional challenge is that we typically only have a *small number of data points per intervention* due to high experimental costs. This renders joint inference over causal structures and interventions brittle, and a rigorous treatment of uncertainty is paramount for reaching

*Correspondence to: alexander.haegle@inf.ethz.ch

reliable conclusions. Recent methods [43, 30, 6, 57] that are able to deal with imperfect or unknown interventions do not account for epistemic uncertainty during inference. Thus, they frequently fail in realistic scenarios where interventional data is scarce.

Addressing these shortcomings, we introduce *Bayesian Causal Discovery with unknown Interventions (BaCaDI)*, a fully Bayesian approach for inferring the complete set of causal structure, functional mechanisms and intervention targets given various unknown experimental/interventional conditions. BaCaDI performs joint inference over causal Bayesian Networks (CBNs) as well as intervention targets and effects across multiple experimental contexts. Our method is fully *differentiable* and operates in the continuous space of latent probabilistic representations of both CBNs and interventions. This makes our approach particularly scalable to causal systems of many variables, and it enables us to approximate complex posteriors via gradient-based particle variational inference.

In a range of experiments with synthetic causal BNs as well as a realistic gene-expression simulator, BaCaDI outperforms related methods in recovering the underlying causal structure and intervention targets. Moreover, the principled treatment of uncertainty allows BaCaDI to provide well-calibrated uncertainty estimates for its predictions, even when the underlying Bayesian model is misspecified as in the case of gene-expression data.

2 Related work

Differentiable optimization for structure learning. Classical algorithms for causal structure learning typically rely on conditional independence tests [56, 55] or combinatorial search [8, 27]. Initiated by Zheng et al. [65], recent works reformulate structure learning as a continuous optimization problem [66, 63, 34, 6], which enables the use of gradient-based learning algorithms for this task. We build on these techniques to obtain continuous relaxations of graphs and enforcing their acyclicity.

Causal discovery from multiple contexts. Learning a causal structure from datasets collected from different interventional contexts of the same causal system has been referred to as Joint Causal Inference (JCI) [43]. Multiple methods handle such combinations of observational and interventional data [40, 64, 23, 60, 62] but assume full knowledge of the interventions. Other methods build on the notion of *invariance* [54, 50, 42, 18, 25, 26], but either do not generalize to full graphs or make restrictive assumptions about the local causal effects.

Causal discovery with unknown interventions. Mooij et al. [43] and Squires et al. [57] reduce the unknown intervention setting to standard causal discovery tools such as conditional independence and invariance tests. However, such hypothesis tests typically require large datasets, making these methods brittle for realistic datasets of small size. Another line of recent work formulates continuous relaxations of the joint inference problem under unknown interventions and uses gradient-based optimization to find the graph and intervention targets [30, 6, 13]. Our approach uses similar ideas to relax the semi-discrete inference problem into a continuous one. However, unlike Ke et al. [30], Brouillard et al. [6], and Faria et al. [13], which only infer point estimates, we adopt a fully Bayesian approach that enables principled uncertainty quantification. Eaton and Murphy [12] is the only work we are aware of that does the same, though only for discrete variables and with a costly dynamic programming approach that does not scale well to larger graphs.

3 Background: Causal Discovery

Causal Bayesian Networks. A Bayesian network (BN) (\mathbf{G}, Θ) uses a directed acyclic graph (DAG) to model the joint density $p(\mathbf{x})$ of d variables $\mathbf{x} = x_{1:d}$ via conditional probabilities. The joint distribution p factorizes as $p(x_1, \dots, x_d | \Theta, \mathbf{G}) = \prod_{i=1}^d p_i(x_i | x_{\text{pa}_{\mathbf{G}}(i)}, \Theta)$ where $\text{pa}_{\mathbf{G}}(i)$ is the set of parents of node i in \mathbf{G} and the parameters Θ describe the exact local conditional distributions. In a *causal* BN (CBN), the edges also describe direct causal relations. For causal structure learning, we assume that there are no hidden confounding variables (causal sufficiency) [46, 56, 47].

Interventions. In the causal graph, an intervention on the variable i corresponds to changing the conditional distribution p_i and replacing it by a new distribution p_i^I . An intervention is typically considered imperfect (soft) if the distribution is changed but the dependence on the causal parents remains, or perfect (hard, structural) if all dependencies to the causal parents are removed, resulting in a mutilated graph \mathbf{G}^{I_k} [e.g. 46, 47].

In this work, we assume the setting of a collection of M interventions $\mathcal{I} := (I_1, \dots, I_M)$, where each intervention $I_k := (I_k^{\text{tar}}, \Theta_{I_k})$ acts on a set of targets $I_k^{\text{tar}} \subseteq \{1, \dots, d\}$. We use Θ_{I_k} to

denote parameters that describe the conditional distributions $p_i^{I_k}(x_i|x_{\text{pa}_{\mathbf{G}}(i)}, \Theta_{I_k})$ induced by the intervention I_k on the target variables $\{x_i | i \in I_k^{\text{tar}}\}$. To keep the notation and following exposition simple, we assume perfect interventions, i.e., $p_i^{I_k}(x_i|x_{\text{pa}_{\mathbf{G}}(i)}, \Theta_{I_k}) = p_i^{I_k}(x_i|\Theta_{I_k})$. However, all the arguments made in the remainder of the paper also hold for soft interventions. The full data distribution under intervention I_k factorizes into the observational and interventional conditionals:

$$p(\mathbf{x}|\Theta, \mathbf{G}, I_k) = \prod_{i \notin I_k} p_i(x_i|x_{\text{pa}_{\mathbf{G}}(i)}, \Theta) \cdot \prod_{i \in I_k} p_i^{I_k}(x_i|\Theta_{I_k}). \quad (1)$$

The local conditional distributions of the variables that are *not* intervened upon do not change with respect to the observational distribution, a principle often referred to as invariance [50] or modularity [47].

Bayesian Inference of BNs. Given i.i.d. observations $\mathcal{D} = \{\mathbf{x}^{(1)}, \dots, \mathbf{x}^{(N)}\}$, Bayesian inference over BNs means constructing a *full posterior* probability density over BNs that model the observations. Following Friedman and Koller [14], given a prior distribution over DAGs $p(\mathbf{G})$ and a prior over BN parameters $p(\Theta|\mathbf{G})$, Bayes' Theorem yields the joint and marginal posterior distributions

$$p(\mathbf{G}, \Theta|\mathcal{D}) \propto p(\mathbf{G})p(\Theta|\mathbf{G})p(\mathcal{D}|\mathbf{G}, \Theta), \quad (2)$$

$$p(\mathbf{G}|\mathcal{D}) \propto p(\mathbf{G})p(\mathcal{D}|\mathbf{G}) \quad (3)$$

where $p(\mathcal{D}|\mathbf{G}) = \int p(\Theta|\mathbf{G})p(\mathcal{D}|\mathbf{G}, \Theta)d\Theta$ is the marginal likelihood. Thus, $p(\mathcal{D}|\mathbf{G})$ in Eq. 3 is only available in closed form for special conjugate cases. The Bayesian formalism allows us to compute expectations of the form

$$\mathbb{E}_{p(\mathbf{G}, \Theta|\mathcal{D})} [f(\mathbf{G}, \Theta)] \quad \text{or} \quad \mathbb{E}_{p(\mathbf{G}|\mathcal{D})} [f(\mathbf{G})] \quad (4)$$

for any function f of interest. For instance, for Bayesian model averaging, we would use $f(\mathbf{G}, \Theta) = p(\mathbf{x}|\mathbf{G}, \Theta)$ or $f(\mathbf{G}) = p(\mathbf{x}|\mathbf{G})$, respectively [38, 39]. In active learning of CBNs, a commonly used f is the information gain in \mathbf{G} from an intervention [59, 44, 9, 1]. Inferring either posterior is computationally challenging since there are $\mathcal{O}(d!2^{\binom{d}{2}})$ possible DAGs with d nodes [51]. Hence, computing the normalization constant $p(\mathcal{D})$ is also generally intractable.

4 Bayesian Causal Discovery with Multi-Context Data

Problem Statement. In this section, we develop a method for Bayesian inference of the causal Bayesian Network (CBN) given *multiple interventional datasets* generated from the same underlying causal model. This setting is also known as learning from multiple contexts [43]. Formally, we are given a set of M datasets $\mathbf{D} = \{\mathcal{D}_1, \dots, \mathcal{D}_M\}$ with corresponding (unknown) interventions $\mathcal{I} = \{I_1, \dots, I_M\}$. Each \mathcal{D}_k is a set of independent samples $\mathcal{D}_k = \{\mathbf{x}^{(k,1)}, \dots, \mathbf{x}^{(k,n_k)}\}$ obtained from the interventional data distribution $p(\mathbf{x}|\Theta_{\text{gt}}, \mathbf{G}_{\text{gt}}, I_k)$ based on the ground truth CBN $(\mathbf{G}_{\text{gt}}, \Theta_{\text{gt}})$. Observational data, if available, can be added to \mathbf{D} as $\mathcal{D}_0 := \mathcal{D}$ with intervention targets $I_0 = \emptyset$.

Our goal is to infer the ground truth CBN $(\mathbf{G}_{\text{gt}}, \Theta_{\text{gt}})$ and interventions \mathcal{I} given the dataset \mathbf{D} . Compared to standard causal inference, the key difficulty is that in addition to the ground truth CBN, the intervention targets I_k^{tar} and their statistical effects Θ_{I_k} are unknown. Therefore, we need to perform joint inference over M mutilated graphs that are all closely connected to an unknown ‘‘prototype’’ graph. Naturally, such inference is well-posed only if the structural changes implied by each intervention I_k are sparse compared to the overall size of \mathbf{G}_{gt} , i.e. $|I_k| \ll d$.

In many relevant application domains such as biology, the observed samples n_k are noisy and small in number. Hence, it is paramount to not only to predict a single prototype CBN alongside one intervention hypothesis per dataset but also to reason about the *epistemic uncertainty* of our empirical inferences. Such uncertainty estimates allow us to quantify the reliability of our predictions and can be used to actively design future experiments. We thus approach the problem from a Bayesian perspective. This renders the task of learning from \mathbf{D} as a posterior inference problem, which we are going to gradually build up in the following.

Known interventions. When the intervention targets I_k^{tar} and the parameters Θ_{I_k} of the intervention effect are known, for $k = 1, \dots, M$, the posterior over CBNs includes (i.) the product of data likelihoods over all datasets in \mathbf{D} , and (ii.) interventional instead of observation likelihoods for $\mathcal{D}_{k \geq 1}$,

$$p(\mathbf{G}, \Theta|\mathbf{D}, \mathcal{I}) \propto \underbrace{p(\mathbf{G})p(\Theta|\mathbf{G})}_{\text{priors}} \underbrace{p(\mathcal{D}_0|\Theta, \mathbf{G})}_{\text{obs. likelihood}} \prod_{k=1}^M \underbrace{p(\mathcal{D}_k|\Theta, \mathbf{G}, I_k)}_{\text{interv. likelihood}}, \quad (5)$$

where $p(\mathcal{D}_k|\Theta, \mathbf{G}, I_k) = \prod_{i=1}^{n_k} p(\mathbf{x}^{(k,i)}|\Theta, \mathbf{G}, I_k)$ is the interventional likelihood for \mathcal{D}_k given $I_k = (I_k^{\text{tar}}, \Theta_{I_k})$.

Unknown interventions. We include unknown interventions in our inference model by introducing additional priors $p(I_k^{\text{tar}})$ and $p(\Theta_{I_k}|I_k^{\text{tar}})$. Accordingly, the modified posterior follows as

$$p(\mathbf{G}, \Theta, \mathcal{I}|\mathbf{D}) \propto \underbrace{p(\mathbf{G})p(\Theta|\mathbf{G})}_{\text{priors}} \underbrace{p(\mathcal{D}_0|\Theta, \mathbf{G})}_{\text{obs. likelihood}} \prod_{k=1}^M \underbrace{p(I_k^{\text{tar}})p(\Theta_{I_k}|I_k^{\text{tar}})}_{\text{interv. priors}} \underbrace{p(\mathcal{D}_k|\Theta, \mathbf{G}, I_k)}_{\text{interv. likelihood}} \quad (6)$$

The prior $p(I_k^{\text{tar}})$ over intervention targets can incorporate prior beliefs about the structure of interventions, e.g. that only a *sparse* set of variables are subject to an intervention at the same time. The parametrization of the interventional distributions $p_i^I(x_i|\Theta_I)$ is informed by the application and reflects the general nature of interventions, e.g., gene knockdowns in biology.

5 A Differentiable Generative Model over CBNs and Interventions

In the following, we represent $\mathbf{G} \in \{0, 1\}^{d \times d}$ as the adjacency matrix and $I_k^{\text{tar}} = [I_{k,1}^{\text{tar}}, \dots, I_{k,d}^{\text{tar}}]^\top \in \{0, 1\}^d$ as the indicator vector where $I_{k,l}^{\text{tar}} = 1$ if the l -th variable is intervened upon and $I_{k,l}^{\text{tar}} = 0$ otherwise. We write \mathcal{I}^{tar} short for the stack $[I_1^{\text{tar}}, \dots, I_M^{\text{tar}}]$ of intervention target masks and $\Theta_{\mathcal{I}} := [\Theta_{I_1}, \dots, \Theta_{I_M}]$ similarly for the intervention effect parameters. As discussed in Sec. 3, the posterior in Eq. 6 is highly intractable as the number of possible DAGs \mathbf{G} grows super-exponentially with the number of variables d . Furthermore, the number of possible intervention targets I_k^{tar} grows in the order of $\mathcal{O}(2^d)$.

To facilitate approximate inference using Eq. 6, we harness recent advances in Bayesian structure learning proposed by Lorch et al. [36] that allows for a *fully differentiable* posterior over graphs. By computing the score of the posterior, we can use approximate inference methods such as variational inference [5] or Stein Variational Gradient Descent (SVGD) [35].

The key idea is to transform the inference problem over discrete structures \mathbf{G} and I_k^{tar} into one over continuous parameters with respect to which we can differentiate. To this end, we introduce continuous latent variables \mathbf{Z} and Γ_k for $k = 1, \dots, M$ that model the generative processes of \mathbf{G} and I_k^{tar} through $p(\mathbf{G}|\mathbf{Z})$ and $p(I_k^{\text{tar}}|\Gamma_k)$. This implies the following factorization of the generative model in Figure 1:

$$p(\mathbf{Z}, \mathbf{G}, \Theta, \Gamma, \mathcal{I}, \mathbf{D}) = \underbrace{p(\mathbf{Z})p(\mathbf{G}|\mathbf{Z})p(\Theta|\mathbf{G})}_{\text{gen. process CBN}} \prod_{k=1}^M \underbrace{p(\Gamma_k)p(I_k^{\text{tar}}|\Gamma_k)p(\Theta_{I_k}|I_k^{\text{tar}})}_{\text{gen. process interv.}} \underbrace{p(\mathcal{D}_k|\mathbf{G}, \Theta, I_k^{\text{tar}}, \Theta_{I_k})}_{\text{interv. likelihood}} \quad (7)$$

where we write $\Gamma := [\Gamma_1, \dots, \Gamma_M]$ for brevity. Under this generative model, it holds that

$$\mathbb{E}_{p(\mathbf{G}, \Theta, \mathcal{I}|\mathbf{D})}[f(\mathbf{G}, \Theta, \mathcal{I})] = \mathbb{E}_{p(\mathbf{Z}, \Theta, \Gamma, \Theta_{\mathcal{I}}|\mathbf{D})} \left[\frac{\mathbb{E}_{p(\mathbf{G}|\mathbf{Z}), p(\mathcal{I}^{\text{tar}}|\Gamma)}[f(\mathbf{G}, \Theta, \mathcal{I})p(\Theta|\mathbf{G})p(\Theta_{\mathcal{I}}|\mathcal{I}^{\text{tar}})p(\mathbf{D}|\mathbf{G}, \mathcal{I}, \Theta)]}{\mathbb{E}_{p(\mathbf{G}|\mathbf{Z}), p(\mathcal{I}^{\text{tar}}|\Gamma)}[p(\Theta|\mathbf{G})p(\Theta_{\mathcal{I}}|\mathcal{I}^{\text{tar}})p(\mathbf{D}|\mathbf{G}, \mathcal{I}, \Theta)]} \right], \quad (8)$$

with $p(\mathbf{D}|\mathbf{G}, \mathcal{I}, \Theta) = \prod_{k=1}^M p(\mathcal{D}_k|\mathbf{G}, \Theta, I_k^{\text{tar}}, \Theta_{I_k})$ and $p(\mathcal{I}|\Gamma) = \prod_{k=1}^M p(I_k^{\text{tar}}|\Gamma_k)p(\Theta_{I_k}|I_k^{\text{tar}})$. A proof is provided in Appx. A.1. Eq. 8 allows us to compute Bayesian expectations under the posterior in Eq. 5 in terms of the posterior $p(\mathbf{Z}, \Theta, \Gamma, \Theta_{\mathcal{I}}|\mathbf{D})$ over parameters that are continuous. Before we discuss how to perform approximate inference with $p(\mathbf{Z}, \Theta, \Gamma, \Theta_{\mathcal{I}}|\mathbf{D})$, we further specify the conditional probabilities of our generative model and how to make them differentiable.

Generative model of DAGs \mathbf{G} . Following Lorch et al. [36], we define the latent variable $\mathbf{Z} = [\mathbf{U}, \mathbf{V}]$ as a stack of two embedding matrices $\mathbf{U}, \mathbf{V} \in \mathbb{R}^{d \times d}$ and the generative model for the adjacency matrix \mathbf{G} by using the inner product between the latent variables in \mathbf{Z} :

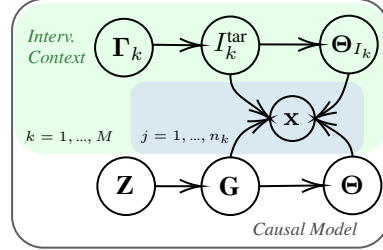


Figure 1: Generative model of combining causal BNs with interventions from different contexts.

$$p_\alpha(\mathbf{G}|\mathbf{Z}) = \prod_{i=1}^d \prod_{j \neq i}^d p_\alpha(g_{ij}|\mathbf{u}_i, \mathbf{v}_j) \quad \text{with} \quad p_\alpha(g_{ij} = 1|\mathbf{u}_i, \mathbf{v}_j) = \sigma_\alpha(\mathbf{u}_i^\top \mathbf{v}_j) \quad (9)$$

where $\sigma_\alpha(x) = 1/(1 + \exp(-\alpha x))$ is the sigmoid function with inverse temperature α and $\mathbf{u}_i, \mathbf{v}_j$ the i -th and j -th column vector of \mathbf{U} and \mathbf{V} , respectively. We denote the matrix of edge probabilities in \mathbf{G} given \mathbf{Z} by $\mathbf{G}_\alpha(\mathbf{Z}) \in [0, 1]^{d \times d}$ with $\mathbf{G}_\alpha(\mathbf{Z})_{ij} := \sigma_\alpha(\mathbf{u}_i^\top \mathbf{v}_j)$. The prior over \mathbf{Z} utilizes (i.) factorized Gaussians with a variance of $\eta_Z^2 = 1/d$ to ensure well-behaved gradients and (ii.) an acyclicity prior that penalizes the expected cyclicity of \mathbf{G} given \mathbf{Z} :

$$p_\beta(\mathbf{Z}) = p(\mathbf{U}, \mathbf{V}) = \underbrace{\exp(-\beta \mathbb{E}_{p(\mathbf{G}|\mathbf{Z})}[h(\mathbf{G})])}_{\text{acyclicity prior}} \prod_{i=1}^d \underbrace{\mathcal{N}(\mathbf{u}_i|\mathbf{0}, \eta_Z^2 \mathbf{I}) \mathcal{N}(\mathbf{v}_i|\mathbf{0}, \eta_Z^2 \mathbf{I})}_{\text{numerical stability}}. \quad (10)$$

Here, β is the inverse temperature parameter controlling how strongly the acyclicity is enforced, and $h(\mathbf{G}) = \text{tr}[(\mathbf{I} + \frac{1}{d}\mathbf{G})^d] - d \geq 0$. We make use of Theorem 1 in Yu et al. [63] states that \mathbf{G} is acyclic iff $h(\mathbf{G}) = 0$. As $\beta \rightarrow \infty$, the support of $p(\mathbf{Z})$ reduces to all \mathbf{Z} that model DAGs [cf. 36].

Generative model of intervention targets \mathcal{I}^{tar} . Similar to the generative model for \mathbf{G} , we define the latent variables $\Gamma \in \mathbb{R}^d$ as the logits of independent Bernoulli distributions that model the entries of the intervention target mask $\mathcal{I}^{\text{tar}} = [I_1^{\text{tar}}, \dots, I_M^{\text{tar}}] \in \{0, 1\}^{M \times d}$:

$$p(\mathcal{I}^{\text{tar}}|\Gamma) = \prod_{k=1}^M \prod_{i=1}^d p_\alpha(I_{k,i}^{\text{tar}}|\gamma_{k,i}) \quad \text{with} \quad p_\alpha(I_{k,i}^{\text{tar}} = 1|\gamma_{k,i}) = \sigma_\alpha(\gamma_{k,i}) \quad (11)$$

We denote the matrix of intervention target probabilities as $\mathcal{I}_\alpha^{\text{tar}}(\Gamma) \in [0, 1]^{M \times d}$ with $\mathcal{I}_\alpha^{\text{tar}}(\Gamma)_{k,i} = \sigma_\alpha(\gamma_{k,i})$. Similar to \mathbf{Z} , the prior over Γ has three components: (i.) A Gaussian term for *numerical stability*, (ii.) a Beta-distribution prior $\text{Beta}(\sigma_\alpha(\gamma_{k,i}); \zeta_1, \zeta_2)$ that encourages $\sigma_\alpha(\gamma_{k,i})$ to be close to 0 or 1, and (iii.) a *sparsity prior* $p_{\text{sparsity}}(\gamma_k) = \exp(-\lambda \|\sigma_\alpha(\gamma_k)\|_1)$ with the l_1 -norm of $\sigma_\alpha(\gamma_k)$ and the inverse temperature parameter λ .

$$p(\Gamma) \propto \prod_{k=1}^M \underbrace{\exp(-\lambda \|\sigma_\alpha(\gamma_k)\|_1)}_{\text{sparse masks}} \prod_{i=1}^d \underbrace{\text{Beta}(\sigma_\alpha(\gamma_{k,i}); \zeta_1, \zeta_2)}_{\text{sharp masks}} \underbrace{\mathcal{N}(\gamma_k|\mathbf{0}, \eta_\gamma^2 \mathbf{I})}_{\text{numerical stability}} \quad (12)$$

We assume that interventions occur only infrequently, i.e., in expectation only on one variable. Hence, we choose $\zeta_1 = 1/d$ and $\zeta_2 = (d-1)/d$. The sparsity prior implies that, given an active intervention target i , it is a-priori less likely that a variable $j \neq i$ is intervened upon in the same context k .

The differentiable interventional likelihood. We obtain a differentiable version of the interventional likelihood by sampling masks $\mathcal{I}^{\text{tar}} \sim \text{Bernoulli}(\sigma_\alpha(\Gamma))$ with the Gumbel-Softmax trick [28, 37] and using them to select between observational and interventional likelihoods per variable:

$$p(\mathcal{D}_k|\mathbf{G}, \Theta, I_k^{\text{tar}}, \Theta_{I_k}) = \prod_{j=1}^{n_k} \prod_{i=1}^d \left(p(x_i^{(k,j)}|x_{\text{pa}_{\mathbf{G}}(i)}, \Theta)^{(1-I_k^{\text{tar}}, i)} \cdot p(x_i^{(k,j)}|\Theta_{I_k})^{I_k^{\text{tar}}, i} \right) \quad (13)$$

Estimating gradients of the log-posterior. While the score w.r.t. parameters Θ and $\Theta_{\mathcal{I}}$ can be obtained in a straightforward manner via automatic differentiation, the score w.r.t. auxiliary variables \mathbf{Z} and Γ requires marginalization over the corresponding discrete structures \mathbf{G} and \mathcal{I}^{tar} as given by

$$\nabla_{\mathbf{Z}} \log p(\mathbf{Z}, \Theta, \Gamma, \Theta_{\mathcal{I}}|\mathbf{D}) = \nabla_{\mathbf{Z}} \log p(\mathbf{Z}) + \frac{\nabla_{\mathbf{Z}} \mathbb{E}_{p(\mathbf{G}|\mathbf{Z})} \mathbb{E}_{p(\mathcal{I}^{\text{tar}}|\Gamma)} [p(\Theta, \Theta_{\mathcal{I}}, \mathbf{D}|\mathbf{G}, \mathcal{I}^{\text{tar}})]}{\mathbb{E}_{p(\mathbf{G}|\mathbf{Z})} \mathbb{E}_{p(\mathcal{I}^{\text{tar}}|\Gamma)} [p(\Theta, \Theta_{\mathcal{I}}, \mathbf{D}|\mathbf{G}, \mathcal{I}^{\text{tar}})]}, \quad (14)$$

$$\nabla_{\Gamma} \log p(\mathbf{Z}, \Theta, \Gamma, \Theta_{\mathcal{I}}|\mathbf{D}) = \nabla_{\Gamma} \log p(\Gamma) + \frac{\nabla_{\Gamma} \mathbb{E}_{p(\mathbf{G}|\mathbf{Z})} \mathbb{E}_{p(\mathcal{I}^{\text{tar}}|\Gamma)} [p(\Theta, \Theta_{\mathcal{I}}, \mathbf{D}|\mathbf{G}, \mathcal{I}^{\text{tar}})]}{\mathbb{E}_{p(\mathbf{G}|\mathbf{Z})} \mathbb{E}_{p(\mathcal{I}^{\text{tar}}|\Gamma)} [p(\Theta, \Theta_{\mathcal{I}}, \mathbf{D}|\mathbf{G}, \mathcal{I}^{\text{tar}})]}. \quad (15)$$

where, $p(\Theta, \Theta_{\mathcal{I}}, \mathbf{D}|\mathbf{G}, \mathcal{I}^{\text{tar}}) = p(\Theta|\mathbf{G}) \prod_{k=1}^m p(\mathcal{D}_k|\mathbf{G}, \Theta, I_k^{\text{tar}}, \Theta_{I_k}) p(\Theta_{I_k}|I_k^{\text{tar}})$. The expectations in Eq. 14 and Eq. 15 can be estimated and differentiated by sampling the intervention masks $\mathcal{I}^{\text{tar}} \sim \text{Bern}(\sigma_\alpha(\Gamma))$ and the adjacency matrices $\mathbf{G} \sim \text{Bern}(\sigma_\alpha(\mathbf{U}\mathbf{V}^\top))$ using the Gumbel-Softmax trick [28, 37]. For obtaining a differentiable log-likelihood, we mask individual log-likelihood summands based on \mathbf{G} [36] and use the intervention masks \mathcal{I}^{tar} to select between observational and interventional log-likelihood (cf. Eq.13).

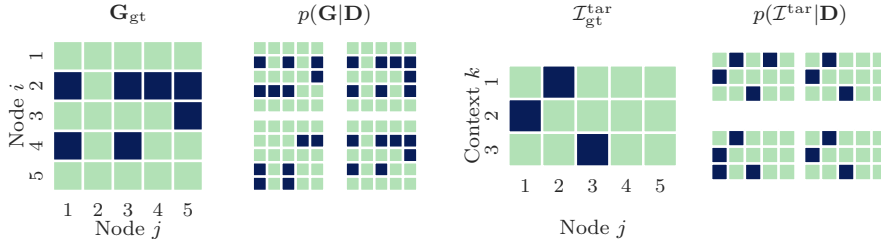


Figure 2: Instead of just one point estimate, BaCaDI yields particle approximations of the posteriors $p(\mathbf{G}|\mathbf{D})$ and $p(\mathcal{I}^{\text{tar}}|\mathbf{D})$. We visually compare the posterior particles with the ground truth \mathbf{G}_{gt} and $\mathcal{I}_{\text{gt}}^{\text{tar}}$ for a SF-2 graph with $d = 5$ nodes and $M = 3$ contexts. Blue colors represent edges or targets.

6 Stein Variational Gradient Descent over CBNs and Interventions

In Section 5, we have introduced a fully differentiable Bayesian framework that translates posterior inference over discrete graphs \mathbf{G} and intervention targets \mathcal{I}_{tar} into an inference problem over the continuous latent variables \mathbf{Z} and $\mathbf{\Gamma}$. In this section, we discuss how to approach the final challenge of approximating the intractable posterior $p(\mathbf{Z}, \mathbf{\Theta}, \mathbf{\Gamma}, \mathbf{\Theta}_{\mathcal{I}}|\mathbf{D})$ over all continuous latent variables.

To this end, we employ the particle variational inference approach SVGD [35], which minimizes the KL divergence to the intractable distribution of interest using a finite set of particles. SVGD depends on the score of the density for guiding the particles towards regions of high probability and a kernel function $k(\cdot, \cdot)$ for introducing a repulsive force between the particles. Refer to Appx. F for an overview of SVGD. We employ a sum of RBF kernels as the kernel function over $\Psi := (\mathbf{Z}, \mathbf{\Theta}, \mathbf{\Gamma}, \mathbf{\Theta}_{\mathcal{I}})$, which performed better than a product kernel composition (see Appx. B.2).

Starting with an initial set of L particles $\{\Psi_0^{(l)}\}_{l=1}^L = \{(\mathbf{Z}_0^{(l)}, \mathbf{\Gamma}_0^{(l)}, \mathbf{\Theta}_0^{(l)}, \mathbf{\Theta}_{\mathcal{I},0}^{(l)})\}_{l=1}^L$, we perform T iterations of particle SVGD updates. Following Lorch et al. [36], we use annealing schedules $\alpha_t \rightarrow \infty$ and $\beta_t \rightarrow \infty$ so that our continuous relaxations $\mathbf{G}_\alpha(\mathbf{Z})$ and $\mathcal{I}_\alpha^{\text{tar}}(\mathbf{\Gamma})$ converge to DAGs and actual sets of intervention targets (details in Appx B.1). We return $\{(\mathbf{G}_\infty(\mathbf{Z}_T^{(l)}), \mathbf{\Theta}_T^{(l)}, \mathcal{I}_\infty^{\text{tar}}(\mathbf{\Gamma}_T^{(l)}), \mathbf{\Theta}_{\mathcal{I},T}^{(l)})\}_{l=1}^L$ as the particle approximation of the posterior $p(\mathbf{G}, \mathbf{\Theta}, \mathcal{I}_{\text{tar}}, \mathbf{\Theta}_{\mathcal{I}}|\mathbf{D})$ with discrete DAGs and interventions targets. Figure 2 illustrates an example of the returned posterior particles for \mathbf{G} and \mathcal{I}_{tar} alongside the ground truth for the case of a linear Gaussian five-node graph. The proposed algorithm is summarized in Algorithm 1 of Appx B. While SVGD yields a set of particles of with equal weights, we weight each particle by its unnormalized posterior probability $p(\mathbf{G}, \mathbf{\Theta}, \mathbf{\Theta}_{\mathcal{I}}, \mathcal{I}_{\text{tar}}|\mathbf{D})$ for performing approximate Bayesian model averaging. We find that this improves the empirical performance.

Although we employ SVGD, our general framework from Sec. 5 can also be instantiated with other score-based sampling [e.g. 61, 7] or variational inference methods [5]. Such alternatives may become favorable for systems of many variables, since the size of the adjacency matrix \mathbf{G} grows quadratically in d and the respective kernel component between \mathbf{G} 's becomes ineffective in high-dimensions.

7 Experiments

We evaluate BaCaDI on different causal discovery tasks with data from multiple contexts. Our goal is to empirically investigate how accurately BaCaDI predicts the causal structure as well as the intervention targets and how it compares to related state-of-the-art methods. First, we focus on synthetic datasets generated by CBNs. Second, we use the SERGIO simulator [10] to evaluate the methods on the more realistic task of simulated gene expression data. Finally, we analyse how well the uncertainty estimates are calibrated.

7.1 Experiment Methodology

Datasets. Following related work [65, 63, 66, 3, 53, 36], we perform inference of randomly sampled graphs with different local conditionals. We consider Erdős-Rényi [19] and scale-free [4] random graphs with $d = 20$ nodes and $2d$ edges in expectation (ER-2 and SF-2). We create datasets by randomly sampling parameters or simulating data with SERGIO. We then split the data into training and held-out test datasets. In all settings, we collect $n_0 = 100$ observational samples together with $n_k = 10$ samples per intervention context for $k \in \{1, \dots, M\}$. This constitutes a low-sample setting commonly found in many applications. Further details on data generation are given in Appx. D.

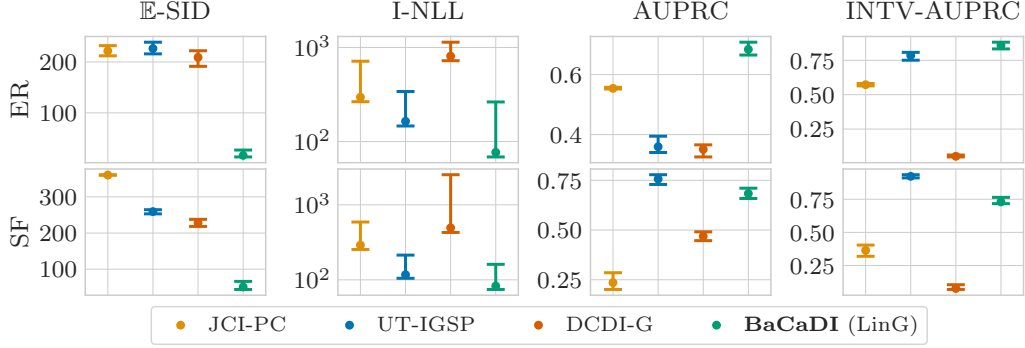


Figure 3: Joint post. inference over CBNs and interventions for *linear Gaussian* ground-truth CBNs. The results are for data from ER-2 and SF-2 graphs with $d = 20$ variables and $M = 20$ contexts.

Baselines. We compare BaCaDI to existing algorithms that are capable of joint causal inference from multiple contexts with unknown interventions. This includes the constraint-based methods UT-IGSP [57] and the JCI framework with the PC algorithm (JCI-PC) [43] and the score-based method DCDI [6], which can handle unknown interventions. JCI-PC and UT-IGSP are based on conditional independence or invariance tests. For DCDI, we use a neural network to model the local conditionals with Gaussian additive noise (DCDI-G). This is the same model class and capacity as BaCaDI with a nonlinear likelihood model. Since all of these methods infer only a single DAG estimate, we use the nonparametric DAG bootstrap approach [15, 1] to obtain an approximate distribution over DAGs and intervention targets.

BaCaDI instantiations. Unless specified otherwise, we model interventions using a Gaussian likelihood $p_i^{I_k}(x_i|\Theta_{I_k}) = \mathcal{N}(x_i|\mu_{k,i}^I, \sigma_I^2)$ with fixed variance $\sigma_I^2 = 0.5$. We infer the means $\Theta_{I_k} = [\mu_{k,1}^I, \dots, \mu_{k,d}^I]$ using a wide Gaussian prior $p(\Theta_{I_k}|I_k^{\text{tar}}) = \prod_{i \in I_k^{\text{tar}}} p(\mu_{k,i}^I|I_{k,i}^{\text{tar}} = 1) = \prod_{i \in I_k^{\text{tar}}} \mathcal{N}(\mu_{k,i}^I|0, 10)$. This reflects an uninformative prior over a large effect range of the interventions. The local conditionals for the observational likelihood are either modelled as linear or nonlinear models with additive Gaussian noise. The latter uses 1 hidden-layer neural networks (NN) with 5 hidden units. More details about the models can be found in Appx. D.1.

Metrics. Our reported metrics focus on three essential aspects of our inference problem: causal graph prediction, intervention detection, and inference of the full CBN for modeling the effects of interventions.

Causal Discovery: We focus on the *Structural Interventional Distance* (SID) [49] that quantifies the closeness between two DAGs in terms of how well their interventional adjustment sets coincide. Since we perform posterior inference and arrive at a distribution over graphs, we consider the *expected SID*: $\mathbb{E}\text{-SID}(p, \mathbf{G}_{\text{gt}}) := \sum_{\mathbf{G}} p(\mathbf{G}|\mathcal{D}) \cdot \text{SID}(\mathbf{G}, \mathbf{G}_{\text{gt}})$. Since UT-IGSP and JCI-PC only return a CPDAGs of the Interventional Markov Equivalence Class (I-MEC), we calculate its lower and upper bound of the SID, and report their midpoint as the $\mathbb{E}\text{-SID}$ (see Appx. D.5). Furthermore, we compute the area under the precision recall curve (AUPRC) for pairwise edge prediction based on the posterior marginals $p(g_{ij} = 1|\mathbf{D})$.

Intervention Targets: We report *interventional AUPRC* (INTV-AUPRC) for the detection of targets.

Predicting the Effects of Interventions: We compute the average negative *interventional log-likelihood* (I-NLL) (see Appx. D.5) on $M^{\text{test}} = 10$ heldout interventional datasets $\mathbf{D}^{\text{test}} = \{\mathcal{D}_1^{\text{test}}, \dots, \mathcal{D}_{10}^{\text{test}}\}$, where different interventions are performed than in the training datasets. Each test dataset comprises 100 samples and has known intervention targets $I_{\text{test},k}^{\text{tar}}$ and effect distributions $p(x_i|\Theta_{I_{\text{test},k}})$. Since UT-IGSP and JCI-PC do not learn the local conditional distributions, we use the closed-form MLE parameters for a linear Gaussian model to compute the heldout I-NLL [24].

Result aggregation. For all methods and settings, we perform a search over a specified range of hyperparameter using at least 20 settings. For a specific choice of hyperparameters, we collect results over 30 different random graphs and pick the hyperparameters that resulted in the lowest I-NLL across the 30 instances in the held-out interventional dataset. We report the median of each metric together with its 90% confidence interval based on the empirical percentiles.

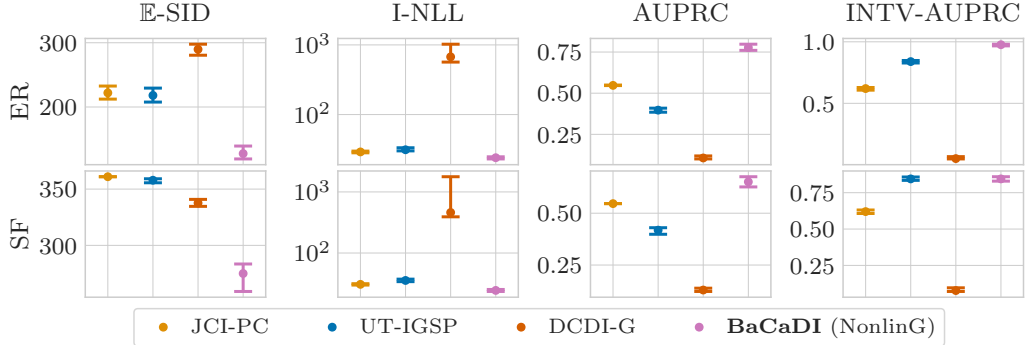


Figure 4: Joint posterior inference over CBNs and interventions for *nonlinear Gaussian* ground-truth CBNs. The results are for data from ER-2 (top) and SF-2 (bottom) graphs with $d = 20$ variables and $M = 20$ contexts. BaCaDI consistently gives the best causal structure and intervention predictions.

7.2 Experiment Results on Synthetic Data

First, we study the performance of BaCaDI and the baselines on joint causal inference from synthetic data. We focus on hard interventions that set the values of the targeted variable to samples from a Gaussian with a randomly chosen mean bounded away from zero and a variance of 0.5. Each interventional dataset is generated by intervening on a specific variable. We target all variables in the graph, i.e., the number of interventional contexts is $M = d$. In total, this results in 300 samples for synthetic datasets with $d = 20$ variables.

We first consider *linear Gaussian* CBNs, where each variable is a linear combination of its parents with additive Gaussian noise. The corresponding results for ER-2 and SF-2 are shown in Fig. 3. As a second task, we evaluate the setting of *nonlinear Gaussian* local conditionals, where the mean of each variable given its parents is described by a neural network (NN) (see Appx. D.2 for details). Fig. 4 displays the results for nonlinear CBNs.

Across these four synthetic evaluation settings, BaCaDI’s causal structure predictions are the closest to the ground-truth CBN a) in terms of their intervention implications, (i.e., E-SID, I-NLL) as well as b) for predicting individual edges, i.e., AUPRC. In most cases, our method outperforms the baselines by a significant margin. Moreover, BaCaDI achieves strong AUPRC scores for the prediction of intervention targets. Among the baselines, UT-IGSP is the best at detecting interventions, largely on par with BaCaDI. Although UT-IGSP also achieves high AUPRC for the linear SF-2 setting, the method performs significantly worse than BaCaDI in other settings and metrics. DCDI performs poorly in predicting the interventions and causal mechanisms. We hypothesize that this is because DCDI neither takes into account epistemic uncertainties nor regularizes its neural network conditionals, making it prone to overfitting in small data settings like ours.

7.3 Experiments on Simulated Gene-Regulatory Networks

We evaluate all methods in a realistic application domain using SERGIO [10], a simulator for single-cell expression data of gene regulatory networks. Given a user-defined causal graph G , SERGIO utilizes stochastic differential equations to simulate the gene expression dynamics and generate realistic single-cell transcriptomic datasets, which correspond to samples from the steady state of this dynamical system. Since real-world gene regulatory networks resemble scale-free structures [2, 45], we use randomly sampled SF-2 graphs with $d = 20$. In this domain, we perform $M = 10$ gene knockout interventions on a single randomly selected target per context, resulting in a dataset size of 200 including the observational samples. See Appx. D.3 for more details.

Our Bayesian formulation allows us to embed prior knowledge into the inference process in a principled manner. In particular, since we perform knockout interventions, we expect intervention values to be close to zero and exhibit low variance. To reflect this prior belief, we set the intervention noise to $\sigma_I^2 = 0.01$ and use the prior $p(\mu_{k,i}^I | I_{k,i}^{\text{tar}} = 1) = \mathcal{N}(\mu_{k,i}^I | 0, 1)$.

Accuracy. Fig. 5 shows the results for the SERGIO datasets. As in the synthetic CBN domain, BaCaDI infers the ground-truth graph most accurately given the provided data. Moreover, it is very accurate in predicting intervention targets as reflected by the intervention target AUPRC score,

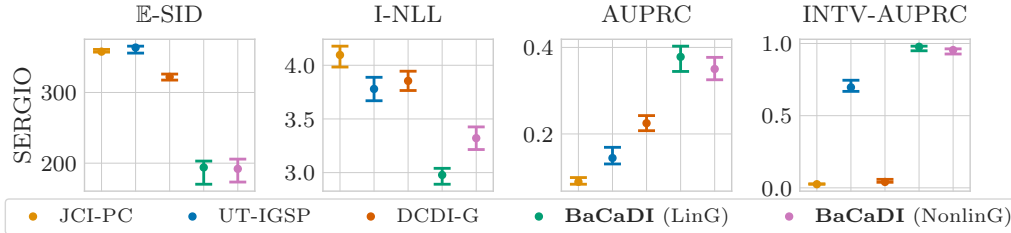


Figure 5: Joint posterior over CBNs and interventions for simulated *gene expression* data with $d = 20$ variables and $M = 10$ interv. contexts. BaCaDI makes significantly better causal mechanism predictions than the baselines and accurately identifies the correct intervention targets.

where it benefits from the prior. In this context, the accuracy of JCI-PC is close to random guessing, predicting nearly no interventions and edges in the CPDAG.

Since the data generated by SERGIO are samples from the steady state of a stochastic dynamical system, our Bayesian model from Sec. 5 is misspecified. The fact that BaCaDI still performs well demonstrates its robustness to model misspecification. Overall, BaCaDI is able to make accurate causal structure predictions with only 200 simulated gene expression measurements from a challenging multi-experiment setting. This is a promising step towards joint causal inference in the life sciences. Here, the predicted intervention targets can further be of independent interest, e.g., for understanding off-target effects of drugs.

Calibration. To quantify the reliability of our uncertainty estimates, we utilize the concept of *calibration* [21, 33]. Formally, we consider a probabilistic predictor to be well calibrated if in expectation, its α -% confidence intervals cover α -% of the true targets.

We visualize this in Fig. 6 for the task of predicting edges in CBNs. The plot compares the confidence intervals for varying thresholds of α with the empirical coverage, that is, the average percentage of edges present in the ground-truth graphs. Perfectly calibrated predictions would exhibit a proportional one-to-one relationship between confidence level and empirical coverage, indicated by the black diagonal line in Fig. 6. All three baseline methods are severely overconfident in their predictions. In contrast, BaCaDI produces edge predictions that are close to the ideal calibration line. This indicates that BaCaDI properly takes into account the *epistemic uncertainty* when dealing with limited data and shows that its probabilistic predictions are reliable. Additionally, BaCaDI offers the possibility to fine-tune the calibration of the predictor through the SVGD kernel parameters. Further analysis of this fine-tuning is given in Appx. E.2.

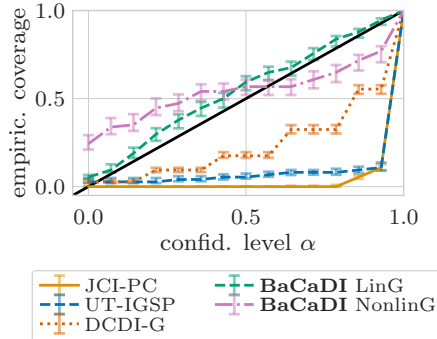


Figure 6: Calibration plot for edge predictions with SERGIO simulated data. Only BaCaDI makes well-calibrated predictions.

8 Conclusion

In this work, we introduced BaCaDI, a fully-differentiable Bayesian causal discovery framework for data generated under various unknown experimental/interventional conditions. BaCaDI performs approximate inference jointly over the underlying causal graph, mechanisms, and the unknown interventions. A key feature of BaCaDI is its principled treatment of epistemic uncertainty, which allows it to operate reliably even when data is scarce, providing well-calibrated uncertainty estimates alongside its structural predictions. Our work is motivated by the challenging problem of inferring the causal mechanisms of gene regulatory networks from real single-cell gene expression data. Our experimental results for the simulated gene expression data in Sec. 7.3 show that BaCaDI brings us one step closer to this ambitious goal. To ultimately reach it, a range of further challenges, such as dealing with the experimental measurement noise incurred by single-cell sequencing techniques, will have to be overcome by future work.

Acknowledgments and Disclosure of Funding

This research was supported by the European Research Council (ERC) under the European Union’s Horizon 2020 research and innovation program grant agreement no. 815943 and the Swiss National Science Foundation under NCCR Automation, grant agreement 51NF40 180545. Jonas Rothfuss was supported by an Apple Scholars in AI/ML fellowship. We thank Parnian Kassraie for valuable feedback.

References

- [1] Raj Agrawal, Chandler Squires, Karren Yang, Karthikeyan Shanmugam, and Caroline Uhler. ABCD-Strategy: Budgeted experimental design for targeted causal structure discovery. In *Proceedings of Machine Learning Research*, volume 89, pages 3400–3409. PMLR, 16–18 Apr 2019.
- [2] Reka Albert. Scale-free networks in cell biology. *Journal of cell science*, 118(21):4947–4957, 2005.
- [3] Yashas Annadani, Jonas Rothfuss, Alexandre Lacoste, Nino Scherrer, Anirudh Goyal, Yoshua Bengio, and Stefan Bauer. Variational causal networks: Approximate bayesian inference over causal structures. *arXiv preprint arXiv:2106.07635*, 2021.
- [4] Albert-László Barabási and Réka Albert. Emergence of scaling in random networks. *Science*, 286(5439):509–512, 1999.
- [5] David M. Blei, Alp Kucukelbir, and Jon D. McAuliffe. Variational inference: A review for statisticians. *Journal of the American Statistical Association*, 112(518):859–877, Apr 2017. ISSN 1537-274X. doi: 10.1080/01621459.2017.1285773. URL <http://dx.doi.org/10.1080/01621459.2017.1285773>.
- [6] Philippe Brouillard, Sébastien Lachapelle, Alexandre Lacoste, Simon Lacoste-Julien, and Alexandre Drouin. Differentiable causal discovery from interventional data, 2020.
- [7] Tianqi Chen, Emily Fox, and Carlos Guestrin. Stochastic Gradient Hamiltonian Monte Carlo. In *International Conference on Machine Learning*, pages 1683–1691. PMLR, 2014.
- [8] David Maxwell Chickering. Optimal structure identification with greedy search. *Journal of Machine Learning Research*, 3(Nov):507–554, 2002.
- [9] Hyunghoon Cho, Bonnie Berger, and Jian Peng. Reconstructing causal biological networks through active learning. *PLoS one*, 11(3):e0150611, 2016.
- [10] Payam Dibaenia and Saurabh Sinha. SERGIO: a single-cell expression simulator guided by gene regulatory networks. *Cell systems*, 11(3):252–271, 2020.
- [11] Dorit Dor and Michael Tarsi. A simple algorithm to construct a consistent extension of a partially oriented graph. *Technical Report R-185, Cognitive Systems Laboratory, UCLA*, 1992.
- [12] Daniel Eaton and Kevin Murphy. Exact bayesian structure learning from uncertain interventions. In *Artificial intelligence and statistics*, pages 107–114. PMLR, 2007.
- [13] Gonçalo RA Faria, André FT Martins, and Mário AT Figueiredo. Differentiable causal discovery under latent interventions. *arXiv preprint arXiv:2203.02336*, 2022.
- [14] Nir Friedman and Daphne Koller. Being Bayesian About Network Structure. A Bayesian Approach to Structure Discovery in Bayesian Networks. *Machine Learning*, 50(1):95–125, January 2003.
- [15] Nir Friedman, Moises Goldszmidt, and Abraham Wyner. Data analysis with Bayesian networks: A bootstrap approach. *arXiv preprint arXiv:1301.6695*, 2013.
- [16] Dan Geiger and David Heckerman. Learning gaussian networks. In *Uncertainty Proceedings 1994*, pages 235–243. Elsevier, 1994.
- [17] Dan Geiger and David Heckerman. Parameter priors for directed acyclic graphical models and the characterization of several probability distributions. *The Annals of Statistics*, 30(5):1412–1440, 2002.
- [18] AmirEmad Ghassami, Saber Salehkaleybar, Negar Kiyavash, and Kun Zhang. Learning causal structures using regression invariance. *Advances in Neural Information Processing Systems*, 30, 2017.
- [19] Edgar N Gilbert. Random graphs. *The Annals of Mathematical Statistics*, 30(4):1141–1144, 1959.

- [20] Xavier Glorot and Yoshua Bengio. Understanding the difficulty of training deep feedforward neural networks. In *Proceedings of the thirteenth international conference on artificial intelligence and statistics*, pages 249–256. JMLR Workshop and Conference Proceedings, 2010.
- [21] Tilmann Gneiting, Fadoua Balabdaoui, and Adrian E Raftery. Probabilistic forecasts, calibration and sharpness. *Journal of the Royal Statistical Society: Series B (Statistical Methodology)*, 69(2):243–268, 2007.
- [22] Marco Grzegorzczak. An introduction to gaussian bayesian networks. In *Systems Biology in Drug Discovery and Development*, pages 121–147. Springer, 2010.
- [23] Alain Hauser and Peter Bühlmann. Characterization and Greedy Learning of Interventional Markov Equivalence Classes of Directed Acyclic Graphs, 2012.
- [24] Alain Hauser and Peter Bühlmann. Jointly interventional and observational data: estimation of interventional markov equivalence classes of directed acyclic graphs. *Journal of the Royal Statistical Society: Series B (Statistical Methodology)*, 77(1):291–318, may 2014. doi: 10.1111/rssb.12071. URL <https://doi.org/10.1111%2Frssb.12071>.
- [25] Christina Heinze-Deml, Jonas Peters, and Nicolai Meinshausen. Invariant causal prediction for nonlinear models. *Journal of Causal Inference*, 6(2), 2018.
- [26] B. Huang, K. Zhang, J. Zhang, J. Ramsey, R. Sanchez-Romero, C. Glymour, and B. Schölkopf. Causal Discovery from Heterogeneous/Nonstationary Data. *Journal of Machine Learning Research*, 21(89):1–53, 2020. URL <http://jmlr.org/papers/v21/19-232.html>.
- [27] Biwei Huang, Kun Zhang, Yizhu Lin, Bernhard Schölkopf, and Clark Glymour. Generalized score functions for causal discovery. In *Proceedings of the 24th ACM SIGKDD International Conference on Knowledge Discovery & Data Mining*, pages 1551–1560, 2018.
- [28] Eric Jang, Shixiang Gu, and Ben Poole. Categorical reparameterization with gumbel-softmax. *arXiv preprint arXiv:1611.01144*, 2016.
- [29] Diviyani Kalainathan and Olivier Goulet. Causal discovery toolbox: Uncover causal relationships in python, 2019. URL <https://arxiv.org/abs/1903.02278>.
- [30] Nan Rosemary Ke, Olexa Bilaniuk, Anirudh Goyal, Stefan Bauer, Hugo Larochelle, Bernhard Schölkopf, Michael C. Mozer, Chris Pal, and Yoshua Bengio. Learning neural causal models from unknown interventions, 2019. URL <https://arxiv.org/abs/1910.01075>.
- [31] Jack Kuipers and Giusi Moffa. The interventional Bayesian Gaussian equivalent score for Bayesian causal inference with unknown soft interventions, 2022. URL <https://arxiv.org/abs/2205.02602>.
- [32] Jack Kuipers, Giusi Moffa, and David Heckerman. Addendum on the scoring of gaussian directed acyclic graphical models. *The Annals of Statistics*, 42(4):1689–1691, 2014.
- [33] Volodymyr Kuleshov, Nathan Fenner, and Stefano Ermon. Accurate uncertainties for deep learning using calibrated regression. In *International Conference on Machine Learning*, pages 2796–2804. PMLR, 2018.
- [34] Sébastien Lachapelle, Philippe Brouillard, Tristan Deleu, and Simon Lacoste-Julien. Gradient-based neural DAG learning. *arXiv preprint arXiv:1906.02226*, 2019.
- [35] Qiang Liu and Dilin Wang. Stein variational gradient descent: A general purpose bayesian inference algorithm. In *Advances in Neural Information Processing*, 2016.
- [36] Lars Lorch, Jonas Rothfuss, Bernhard Schölkopf, and Andreas Krause. DiBS: Differentiable Bayesian Structure Learning, 2021.
- [37] Chris J. Maddison, Andriy Mnih, and Yee Whye Teh. The concrete distribution: A continuous relaxation of discrete random variables. In *Proceedings International Conference on Learning Representations*, 2017.
- [38] David Madigan and Adrian E Raftery. Model selection and accounting for model uncertainty in graphical models using occam’s window. *Journal of the American Statistical Association*, 89(428):1535–1546, 1994.
- [39] David Madigan, Jonathan Gavrin, and Adrian E Raftery. Eliciting prior information to enhance the predictive performance of bayesian graphical models. *Communications in Statistics-Theory and Methods*, 24(9):2271–2292, 1995.
- [40] Sara Magliacane, Tom Claassen, and Joris M Mooij. Ancestral causal inference. *Advances in Neural Information Processing Systems*, 29, 2016.

- [41] James M McFarland, Brenton R Paoella, Allison Warren, Kathryn Geiger-Schuller, Tsukasa Shibue, Michael Rothberg, Olena Kuksenko, William N Colgan, Andrew Jones, Emily Chambers, et al. Multiplexed single-cell transcriptional response profiling to define cancer vulnerabilities and therapeutic mechanism of action. *Nature communications*, 11(1):1–15, 2020.
- [42] Nicolai Meinshausen, Alain Hauser, Joris M Mooij, Jonas Peters, Philip Versteeg, and Peter Bühlmann. Methods for causal inference from gene perturbation experiments and validation. *Proceedings of the National Academy of Sciences*, 113(27):7361–7368, 2016.
- [43] Joris M. Mooij, Sara Magliacane, and Tom Claassen. Joint Causal Inference from Multiple Contexts. 2016. doi: 10.48550/ARXIV.1611.10351. URL <https://arxiv.org/abs/1611.10351>.
- [44] Kevin P Murphy. Active learning of causal bayes net structure. 2001.
- [45] Wilberforce Zachary Ouma, Katja Pogacar, and Erich Grotewold. Topological and statistical analyses of gene regulatory networks reveal unifying yet quantitatively different emergent properties. *PLoS computational biology*, 14(4):e1006098, 2018.
- [46] Judea Pearl. *Causality*. Cambridge University Press, 2 edition, 2009. doi: 10.1017/CBO9780511803161.
- [47] J. Peters, D. Janzing, and B. Schölkopf. *Elements of Causal Inference: Foundations and Learning Algorithms*. MIT Press, Cambridge, MA, USA, 2017.
- [48] Jonas Peters and Peter Bühlmann. Identifiability of Gaussian structural equation models with equal error variances. *Biometrika*, 101(1):219–228, 2014.
- [49] Jonas Peters and Peter Bühlmann. Structural intervention distance for evaluating causal graphs. *Neural computation*, 27(3):771–799, 2015.
- [50] Jonas Peters, Peter Bühlmann, and Nicolai Meinshausen. Causal inference by using invariant prediction: identification and confidence intervals. *Journal of the Royal Statistical Society. Series B (Statistical Methodology)*, pages 947–1012, 2016.
- [51] R.W. Robinson. Counting labeled acyclic digraphs. *New Directions in the Theory of Graphs*, 1973.
- [52] Thomas Schaffter, Daniel Marbach, and Dario Floreano. GeneNetWeaver: in silico benchmark generation and performance profiling of network inference methods. *Bioinformatics*, 27(16):2263–2270, 06 2011. ISSN 1367-4803. doi: 10.1093/bioinformatics/btr373. URL <https://doi.org/10.1093/bioinformatics/btr373>.
- [53] Nino Scherrer, Olexa Bilaniuk, Yashas Annadani, Anirudh Goyal, Patrick Schwab, Bernhard Schölkopf, Michael C Mozer, Yoshua Bengio, Stefan Bauer, and Nan Rosemary Ke. Learning neural causal models with active interventions. *arXiv preprint arXiv:2109.02429*, 2021.
- [54] B. Schölkopf, D. Janzing, J. Peters, E. Sgouritsa, K. Zhang, and J. M. Mooij. On causal and anticausal learning. In *Proceedings of the 29th International Conference on Machine Learning (ICML)*, pages 1255–1262, 2012.
- [55] Liam Solus, Yuhao Wang, Lenka Matejovicova, and Caroline Uhler. Consistency guarantees for permutation-based causal inference algorithms. *arXiv preprint arXiv:1702.03530*, 2017.
- [56] Peter Spirtes, Clark N Glymour, Richard Scheines, and David Heckerman. *Causation, prediction, and search*. MIT press, 2000.
- [57] Chandler Squires, Yuhao Wang, and Caroline Uhler. Permutation-Based Causal Structure Learning with Unknown Intervention Targets, 2020.
- [58] Sanjay R Srivatsan, José L McFaline-Figueroa, Vijay Ramani, Lauren Saunders, Junyue Cao, Jonathan Packer, Hannah A Pliner, Dana L Jackson, Riza M Daza, Lena Christiansen, et al. Massively multiplex chemical transcriptomics at single-cell resolution. *Science*, 367(6473):45–51, 2020.
- [59] Simon Tong and Daphne Koller. Active learning for structure in bayesian networks. In *International Joint Conference on Artificial Intelligence*, volume 17, pages 863–869, 2001.
- [60] Yuhao Wang, Liam Solus, Karren Yang, and Caroline Uhler. Permutation-based causal inference algorithms with interventions. *Advances in Neural Information Processing Systems*, 30, 2017.
- [61] Max Welling and Yee Whye Teh. Bayesian Learning via Stochastic Gradient Langevin Dynamics. In *International Conference on Machine Learning*, page 681–688, 2011.

- [62] Karren Yang, Abigail Katcoff, and Caroline Uhler. Characterizing and learning equivalence classes of causal dags under interventions. In *International Conference on Machine Learning*, pages 5541–5550. PMLR, 2018.
- [63] Yue Yu, Jie Chen, Tian Gao, and Mo Yu. DAG-GNN: DAG structure learning with graph neural networks. In *International Conference on Machine Learning*, pages 7154–7163. PMLR, 2019.
- [64] Kun Zhang, Biwei Huang, Jiji Zhang, Clark Glymour, and Bernhard Schölkopf. Causal Discovery from Nonstationary/Heterogeneous Data: Skeleton Estimation and Orientation Determination. In *Proceedings of the Twenty-Sixth International Joint Conference on Artificial Intelligence, IJCAI-17*, pages 1347–1353, 2017. doi: 10.24963/ijcai.2017/187. URL <https://doi.org/10.24963/ijcai.2017/187>.
- [65] Xun Zheng, Bryon Aragam, Pradeep Ravikumar, and Eric P. Xing. DAGs with NO TEARS: Continuous Optimization for Structure Learning, 2018.
- [66] Xun Zheng, Chen Dan, Bryon Aragam, Pradeep Ravikumar, and Eric Xing. Learning sparse nonparametric DAGs. In *International Conference on Artificial Intelligence and Statistics*, pages 3414–3425. PMLR, 2020.

A Proofs

A.1 Latent Posterior Expectation

Recall that we have the generative model under which we factorize

$$p(\mathbf{Z}, \mathbf{G}, \Theta, \Gamma, \mathcal{I}, \mathbf{D}) = \underbrace{p(\mathbf{Z})p(\mathbf{G}|\mathbf{Z})p(\Theta|\mathbf{G})}_{\text{gen. process CBN}} \prod_{k=1}^M \underbrace{p(\Gamma_k)p(I_k^{\text{tar}}|\Gamma_k)p(\Theta_{I_k}|I_k^{\text{tar}})}_{\text{gen. process interv.}} \underbrace{p(\mathcal{D}_k|\mathbf{G}, \Theta, I_k^{\text{tar}}, \Theta_{I_k})}_{\text{interv. likelihood}}$$

where we write $\Gamma := [\Gamma_1, \dots, \Gamma_M]$. For brevity, we can express this as

$$p(\mathbf{Z}, \mathbf{G}, \Theta, \Gamma, \mathcal{I}, \mathbf{D}) = p(\mathbf{Z})p(\mathbf{G}|\mathbf{Z})p(\Theta|\mathbf{G}) \cdot p(\Gamma)p(\mathcal{I}^{\text{tar}}|\Gamma)p(\Theta_{\mathcal{I}}|\mathcal{I}^{\text{tar}}) \cdot p(\mathbf{D}|\mathbf{G}, \mathcal{I}, \Theta)$$

where $p(\mathbf{D}|\mathbf{G}, \mathcal{I}, \Theta) = p(\mathbf{D}|\mathbf{G}, \Theta, \mathcal{I}^{\text{tar}}, \Theta_{\mathcal{I}}) = \prod_{k=1}^M p(\mathcal{D}_k|\mathbf{G}, \Theta, I_k^{\text{tar}}, \Theta_{I_k})$.

This gives us

$$\begin{aligned} & \mathbb{E}_{p(\mathbf{G}, \Theta, \mathcal{I}|\mathbf{D})}[f(\mathbf{G}, \Theta, \mathcal{I})] \\ &= \sum_{\mathbf{G}} \int_{\Theta} \sum_{\mathcal{I}^{\text{tar}}} \int_{\Theta_{\mathcal{I}}} p(\mathbf{G}, \Theta, \mathcal{I}|\mathbf{D}) f(\mathbf{G}, \Theta, \mathcal{I}) d\Theta d\Theta_{\mathcal{I}} \\ &= \sum_{\mathbf{G}} \int_{\Theta} \sum_{\mathcal{I}^{\text{tar}}} \int_{\Theta_{\mathcal{I}}} p(\mathbf{G}, \mathcal{I}^{\text{tar}}, \Theta, \Theta_{\mathcal{I}}|\mathbf{D}) f(\mathbf{G}, \Theta, \mathcal{I}) d\Theta d\Theta_{\mathcal{I}} \\ & \text{(splitting } \mathcal{I} \text{ to } \mathcal{I}^{\text{tar}}, \Theta_{\mathcal{I}}) \\ &= \sum_{\mathbf{G}} \int_{\Theta} \sum_{\mathcal{I}^{\text{tar}}} \int_{\Theta_{\mathcal{I}}} \frac{p(\mathbf{G}, \mathcal{I}^{\text{tar}}, \Theta, \Theta_{\mathcal{I}}, \mathbf{D}) f(\mathbf{G}, \Theta, \mathcal{I})}{p(\mathbf{D})} d\Theta d\Theta_{\mathcal{I}} \\ &= \sum_{\mathbf{G}} \int_{\Theta} \sum_{\mathcal{I}^{\text{tar}}} \int_{\Theta_{\mathcal{I}}} \int_{\mathbf{Z}} \int_{\Gamma} \frac{p(\mathbf{Z}, \mathbf{G}, \Gamma, \mathcal{I}^{\text{tar}}, \Theta, \Theta_{\mathcal{I}}, \mathbf{D}) f(\mathbf{G}, \Theta, \mathcal{I})}{p(\mathbf{D})} d\mathbf{Z} d\Gamma d\Theta d\Theta_{\mathcal{I}} \\ & \text{(extending by } \mathbf{Z}, \Gamma) \\ &= \int_{\mathbf{Z}, \Gamma, \Theta, \Theta_{\mathcal{I}}} \sum_{\mathbf{G}, \mathcal{I}^{\text{tar}}} \frac{p(\mathbf{Z}, \mathbf{G}, \Gamma, \mathcal{I}^{\text{tar}}, \Theta, \Theta_{\mathcal{I}}, \mathbf{D}) f(\mathbf{G}, \Theta, \mathcal{I})}{p(\mathbf{D})} d\mathbf{Z} d\Gamma d\Theta d\Theta_{\mathcal{I}} \\ & \text{(rearranging)} \\ &= \int_{\mathbf{Z}, \Gamma, \Theta, \Theta_{\mathcal{I}}} \sum_{\mathbf{G}, \mathcal{I}^{\text{tar}}} \frac{p(\mathbf{Z})p(\mathbf{G}|\mathbf{Z})p(\Theta|\mathbf{G})p(\Gamma)p(\mathcal{I}^{\text{tar}}|\Gamma)p(\Theta_{\mathcal{I}}|\mathcal{I}^{\text{tar}})p(\mathbf{D}|\mathbf{G}, \mathcal{I}, \Theta) f(\mathbf{G}, \Theta, \mathcal{I})}{p(\mathbf{D})} d\mathbf{Z} d\Gamma d\Theta d\Theta_{\mathcal{I}} \\ & \text{(by the generative model)} \\ &= E_{p(\mathbf{Z}, \Theta, \Gamma, \Theta_{\mathcal{I}}|\mathbf{D})} \left[\sum_{\mathbf{G}, \mathcal{I}^{\text{tar}}} \frac{p(\mathbf{G}|\mathbf{Z})p(\Theta|\mathbf{G})p(\mathcal{I}^{\text{tar}}|\Gamma)p(\Theta_{\mathcal{I}}|\mathcal{I}^{\text{tar}})p(\mathbf{D}|\mathbf{G}, \mathcal{I}, \Theta) f(\mathbf{G}, \Theta, \mathcal{I})}{p(\Theta, \Theta_{\mathcal{I}}, \mathbf{D}|\mathbf{Z}, \Gamma)} \right] \\ & \text{(since } p(\mathbf{Z}, \Theta, \Gamma, \Theta_{\mathcal{I}}|\mathbf{D}) = \frac{p(\mathbf{Z})p(\Gamma)p(\Theta, \Theta_{\mathcal{I}}, \mathbf{D}|\mathbf{Z}, \Gamma)}{p(\mathbf{D})}) \\ &= E_{p(\mathbf{Z}, \Theta, \Gamma, \Theta_{\mathcal{I}}|\mathbf{D})} \left[\frac{\sum_{\mathbf{G}, \mathcal{I}^{\text{tar}}} p(\mathbf{G}|\mathbf{Z})p(\Theta|\mathbf{G})p(\mathcal{I}^{\text{tar}}|\Gamma)p(\Theta_{\mathcal{I}}|\mathcal{I}^{\text{tar}})p(\mathbf{D}|\mathbf{G}, \mathcal{I}, \Theta) f(\mathbf{G}, \Theta, \mathcal{I})}{p(\Theta, \Theta_{\mathcal{I}}, \mathbf{D}|\mathbf{Z}, \Gamma)} \right] \\ & \text{(rearranging)} \\ &= E_{p(\mathbf{Z}, \Theta, \Gamma, \Theta_{\mathcal{I}}|\mathbf{D})} \left[\frac{\sum_{\mathbf{G}, \mathcal{I}^{\text{tar}}} p(\mathbf{G}|\mathbf{Z})p(\Theta|\mathbf{G})p(\mathcal{I}^{\text{tar}}|\Gamma)p(\Theta_{\mathcal{I}}|\mathcal{I}^{\text{tar}})p(\mathbf{D}|\mathbf{G}, \mathcal{I}, \Theta) f(\mathbf{G}, \Theta, \mathcal{I})}{\sum_{\mathbf{G}, \mathcal{I}^{\text{tar}}} p(\mathbf{G}, \mathcal{I}^{\text{tar}}, \Theta, \Theta_{\mathcal{I}}, \mathbf{D}|\mathbf{Z}, \Gamma)} \right] \\ & \text{(law of total probability)} \\ &= \mathbb{E}_{p(\mathbf{Z}, \Theta, \Gamma, \Theta_{\mathcal{I}}|\mathbf{D})} \left[\frac{\sum_{\mathbf{G}, \mathcal{I}^{\text{tar}}} p(\mathbf{G}|\mathbf{Z})p(\Theta|\mathbf{G})p(\mathcal{I}^{\text{tar}}|\Gamma)p(\Theta_{\mathcal{I}}|\mathcal{I}^{\text{tar}})p(\mathbf{D}|\mathbf{G}, \mathcal{I}, \Theta) f(\mathbf{G}, \Theta, \mathcal{I})}{\sum_{\mathbf{G}, \mathcal{I}^{\text{tar}}} p(\mathbf{G}|\mathbf{Z})p(\Theta|\mathbf{G})p(\mathcal{I}^{\text{tar}}|\Gamma)p(\Theta_{\mathcal{I}}|\mathcal{I}^{\text{tar}})p(\mathbf{D}|\mathbf{G}, \mathcal{I}, \Theta)} \right] \\ & \text{(by the generative model)} \end{aligned}$$

$$= \mathbb{E}_{p(\mathbf{Z}, \Theta, \Gamma, \Theta_{\mathcal{I}} | \mathbf{D})} \left[\frac{\mathbb{E}_{p(\mathbf{G} | \mathbf{Z}), p(\mathcal{I}^{\text{tar}} | \Gamma)} [f(\mathbf{G}, \Theta, \mathcal{I}) p(\Theta | \mathbf{G}) p(\Theta_{\mathcal{I}} | \mathcal{I}^{\text{tar}}) p(\mathbf{D} | \mathbf{G}, \mathcal{I}, \Theta)]}{\mathbb{E}_{p(\mathbf{G} | \mathbf{Z}), p(\mathcal{I}^{\text{tar}} | \Gamma)} [p(\Theta | \mathbf{G}) p(\Theta_{\mathcal{I}} | \mathcal{I}^{\text{tar}}) p(\mathbf{D} | \mathbf{G}, \mathcal{I}, \Theta)]} \right]$$

A.2 Scores

We will derive the gradients of the unnormalized posterior since

$$\nabla_{\mathbf{Z}} \log p(\mathbf{Z}, \Gamma, \Theta, \Theta_{\mathcal{I}} | \mathcal{D}) = \nabla_{\mathbf{Z}} \log p(\mathbf{Z}, \Gamma, \Theta, \Theta_{\mathcal{I}}, \mathcal{D}) - \nabla_{\mathbf{Z}} \log p(\mathcal{D}) \quad (16)$$

$$= \nabla_{\mathbf{Z}} \log p(\mathbf{Z}, \Gamma, \Theta, \Theta_{\mathcal{I}}, \mathcal{D}) \quad (17)$$

and analogously for the gradients w.r.t. to other variables $\mathbf{Z}, \Gamma, \Theta, \Theta_{\mathcal{I}}$.

By basic rules of probability theory and using the identity $\nabla_{\mathbf{x}} \log p(\mathbf{x}) = \nabla_{\mathbf{x}} p(\mathbf{x}) / p(\mathbf{x})$, we obtain

$$\nabla_{\mathbf{Z}} \log p(\mathbf{Z}, \Gamma, \Theta, \Theta_{\mathcal{I}}, \mathbf{D}) = \quad (18)$$

$$= \nabla_{\mathbf{Z}} \log p(\mathbf{Z}) + \nabla_{\mathbf{Z}} \log p(\Theta, \Theta_{\mathcal{I}}, \mathbf{D} | \mathbf{Z}, \Gamma) \quad (19)$$

$$= \nabla_{\mathbf{Z}} \log p(\mathbf{Z}) + \frac{\nabla_{\mathbf{Z}} p(\Theta, \Theta_{\mathcal{I}}, \mathbf{D} | \mathbf{Z}, \Gamma)}{p(\Theta, \Theta_{\mathcal{I}}, \mathbf{D} | \mathbf{Z}, \Gamma)} \quad (20)$$

$$= \nabla_{\mathbf{Z}} \log p(\mathbf{Z}) + \frac{\nabla_{\mathbf{Z}} [\sum_{\mathbf{G}} \sum_{\mathcal{I}^{\text{tar}}} p(\mathbf{G} | \mathbf{Z}) p(\mathcal{I}^{\text{tar}} | \Gamma) p(\Theta, \Theta_{\mathcal{I}}, \mathbf{D} | \mathbf{G}, \mathcal{I}^{\text{tar}})]}{\sum_{\mathbf{G}} \sum_{\mathcal{I}^{\text{tar}}} p(\mathbf{G} | \mathbf{Z}) p(\mathcal{I}^{\text{tar}} | \Gamma) p(\Theta, \Theta_{\mathcal{I}}, \mathbf{D} | \mathbf{G}, \mathcal{I}^{\text{tar}})} \quad (21)$$

$$= \nabla_{\mathbf{Z}} \log p(\mathbf{Z}) + \frac{\nabla_{\mathbf{Z}} \mathbb{E}_{p(\mathbf{G} | \mathbf{Z})} \mathbb{E}_{p(\mathcal{I}^{\text{tar}} | \Gamma)} [p(\Theta, \Theta_{\mathcal{I}}, \mathbf{D} | \mathbf{G}, \mathcal{I}^{\text{tar}})]}{\mathbb{E}_{p(\mathbf{G} | \mathbf{Z})} \mathbb{E}_{p(\mathcal{I}^{\text{tar}} | \Gamma)} [p(\Theta, \Theta_{\mathcal{I}}, \mathbf{D} | \mathbf{G}, \mathcal{I}^{\text{tar}})]} \quad (22)$$

and analogously

$$\nabla_{\Gamma} \log p(\mathbf{Z}, \Gamma, \Theta, \Theta_{\mathcal{I}}, \mathbf{D}) = \quad (23)$$

$$= \nabla_{\Gamma} \log p(\Gamma) + \nabla_{\Gamma} \log p(\Theta, \Theta_{\mathcal{I}}, \mathbf{D} | \mathbf{Z}, \Gamma) \quad (24)$$

$$= \nabla_{\Gamma} \log p(\Gamma) + \frac{\nabla_{\Gamma} p(\Theta, \Theta_{\mathcal{I}}, \mathbf{D} | \mathbf{Z}, \Gamma)}{p(\Theta, \Theta_{\mathcal{I}}, \mathbf{D} | \mathbf{Z}, \Gamma)} \quad (25)$$

$$= \nabla_{\Gamma} \log p(\Gamma) + \frac{\nabla_{\Gamma} [\sum_{\mathbf{G}} \sum_{\mathcal{I}^{\text{tar}}} p(\mathbf{G} | \mathbf{Z}) p(\mathcal{I}^{\text{tar}} | \Gamma) p(\Theta, \Theta_{\mathcal{I}}, \mathbf{D} | \mathbf{G}, \mathcal{I}^{\text{tar}})]}{\sum_{\mathbf{G}} \sum_{\mathcal{I}^{\text{tar}}} p(\mathbf{G} | \mathbf{Z}) p(\mathcal{I}^{\text{tar}} | \Gamma) p(\Theta, \Theta_{\mathcal{I}}, \mathbf{D} | \mathbf{G}, \mathcal{I}^{\text{tar}})} \quad (26)$$

$$= \nabla_{\Gamma} \log p(\Gamma) + \frac{\nabla_{\Gamma} \mathbb{E}_{p(\mathbf{G} | \mathbf{Z})} \mathbb{E}_{p(\mathcal{I}^{\text{tar}} | \Gamma)} [p(\Theta, \Theta_{\mathcal{I}}, \mathbf{D} | \mathbf{G}, \mathcal{I}^{\text{tar}})]}{\mathbb{E}_{p(\mathbf{G} | \mathbf{Z})} \mathbb{E}_{p(\mathcal{I}^{\text{tar}} | \Gamma)} [p(\Theta, \Theta_{\mathcal{I}}, \mathbf{D} | \mathbf{G}, \mathcal{I}^{\text{tar}})]} . \quad (27)$$

B Algorithm Details

B.1 Annealing of α and β

The latent variables \mathbf{Z} and Γ probabilistically model the causal graph \mathbf{G} and intervention target masks \mathcal{I}^{tar} . In a similar way, they can be viewed as continuous relaxations of \mathbf{G} and \mathcal{I}^{tar} respectively, where the α trades-off between smoothness and accuracy of these relaxations. If $\alpha \rightarrow \infty$, the sigmoid $\sigma_{\alpha}(\cdot)$ converges to the unit step function so that the probability distributions $p(\mathbf{G} | \mathbf{Z})$ and $p(\mathcal{I}^{\text{tar}} | \Gamma)$ become deterministic indicator functions, representing only single discrete graph $\mathbf{G}_{\infty}(\mathbf{Z}) \in \{0, 1\}^{d \times d}$ and target mask $\mathcal{I}_{\infty}^{\text{tar}}(\Gamma) \in \{0, 1\}^{M \times d}$. To be able to make this simplification, as proposed in Lorch et al. [36], we anneal α_t such that $\alpha_t \rightarrow \infty$ and, at terminal iteration of the SVGD training loop, convert \mathbf{Z} and Γ into their discrete counterparts $\mathbf{G}_{\infty}(\mathbf{Z})$ and $\mathcal{I}_{\infty}^{\text{tar}}(\Gamma)$. Similarly, we set an annealing schedule $\beta_t \rightarrow \infty$ for inverse temperature parameter in the latent prior $p_{\beta}(\mathbf{Z})$ such that and we only model DAGs as the training progresses.

Importantly, this annealing process simplifies the expectation in Eq. 8 to

$$\begin{aligned} & \mathbb{E}_{p(\mathbf{G}, \Theta, \mathcal{I} | \mathbf{D})} [f(\mathbf{G}, \Theta, \mathcal{I})] \\ &= \mathbb{E}_{p(\mathbf{Z}, \Theta, \Gamma, \Theta_{\mathcal{I}} | \mathbf{D})} \left[\frac{\mathbb{E}_{p(\mathbf{G} | \mathbf{Z}), p(\mathcal{I}^{\text{tar}} | \Gamma)} [f(\mathbf{G}, \Theta, \mathcal{I}) p(\Theta | \mathbf{G}) p(\Theta_{\mathcal{I}} | \mathcal{I}^{\text{tar}}) p(\mathbf{D} | \mathbf{G}, \mathcal{I}, \Theta)]}{\mathbb{E}_{p(\mathbf{G} | \mathbf{Z}), p(\mathcal{I}^{\text{tar}} | \Gamma)} [p(\Theta | \mathbf{G}) p(\Theta_{\mathcal{I}} | \mathcal{I}^{\text{tar}}) p(\mathbf{D} | \mathbf{G}, \mathcal{I}, \Theta)]} \right] \quad (28) \end{aligned}$$

$$\rightarrow \mathbb{E}_{p(\mathbf{Z}, \Theta, \Gamma, \Theta_{\mathcal{I}} | \mathbf{D})} [f(\mathbf{G}_{\infty}, \Theta, \mathcal{I}_{\infty})],$$

Algorithm 1 BaCaDI with SVGD for inference of $p(\mathbf{G}, \Theta, \mathcal{I}^{\text{tar}}, \Theta_{\mathcal{I}}|\mathbf{D})$

Input: Set of datasets $\mathbf{D} = \{\mathcal{D}_0, \dots, \mathcal{D}_M\}$ from the same causal system under different contexts

Input: Kernel k , schedules for α_t, β_t , and stepsizes η_t

Output: Set of CBN and intervention particles $\{(\mathbf{G}^{(l)}, \Theta^{(l)}, \mathcal{I}^{\text{tar},(l)}, \Theta_{\mathcal{I}}^{(l)})\}_{l=1}^L$

- 1: Initialize set of latent and parameter particles $\{\Psi_0^{(l)}\}_{l=1}^L = \{(\mathbf{Z}_0^{(l)}, \Gamma_0^{(l)}, \Theta_0^{(l)}, \Theta_{\mathcal{I},0}^{(l)})\}_{l=1}^L$
 - 2: **for** iteration $t = 0$ to $T - 1$ **do**
 - 3: Estimate $\nabla \log p(\mathbf{Z}, \Theta, \Gamma, \Theta_{\mathcal{I}}|\mathbf{D})$ for each $\Psi_t^{(l)} = (\mathbf{Z}_t^{(l)}, \Theta_t^{(l)}, \Gamma_t^{(l)}, \Theta_{\mathcal{I},t}^{(l)})$ \triangleright see Eq 14, 15
 - 4: **for** particle $m = l$ to L **do**
 - 5: $\mathbf{Z}_{t+1}^{(l)} \leftarrow \mathbf{Z}_t^{(l)} + \eta_t \phi_t^{\mathbf{Z}}(\Psi_t^{(l)})$ \triangleright SVGD steps
 where $\phi_t^{\mathbf{Z}}(\cdot) := \frac{1}{L} \sum_{l=L}^M \left[k(\Psi_t^{(l)}, \cdot) \nabla_{\mathbf{Z}_t^{(l)}} \log p(\Psi_t^{(l)}|\mathbf{D}) + \nabla_{\mathbf{Z}_t^{(l)}} k(\Psi_t^{(l)}, \cdot) \right]$
 - 6: $\Theta_{t+1}^{(l)} \leftarrow \Theta_t^{(l)} + \eta_t \phi_t^{\Theta}(\Psi_t^{(l)})$
 - 7: $\Gamma_{t+1}^{(l)} \leftarrow \Gamma_t^{(l)} + \eta_t \phi_t^{\Gamma}(\Psi_t^{(l)})$
 - 8: $\Theta_{\mathcal{I},t+1}^{(l)} \leftarrow \Theta_{\mathcal{I},t}^{(l)} + \eta_t \phi_t^{\Theta_{\mathcal{I}}}(\Psi_t^{(l)})$
 where $\phi_t^{\Theta}, \phi_t^{\Gamma}, \phi_t^{\Theta_{\mathcal{I}}}$ are analogous to $\phi_t^{\mathbf{Z}}$ but use gradients $\nabla_{\Theta_t^{(l)}}, \nabla_{\Gamma_t^{(l)}}, \nabla_{\Theta_{\mathcal{I},t}^{(l)}}$
 - 9: **return** $\{(\mathbf{G}_{\infty}(\mathbf{Z}_T^{(l)}), \Theta_T^{(l)}, \mathcal{I}_{\infty}^{\text{tar}}(\Gamma_T^{(l)}), \Theta_{\mathcal{I},T}^{(l)})\}_{l=1}^L$ \triangleright see Appx. B.1
-

where $\mathcal{I}_{\infty} := (\mathcal{I}_{\infty}^{\text{tar}}(\Gamma), \Theta_{\mathcal{I}})$. This holds since the inner expectations evaluate to a single point for $\alpha_t, \beta_t \rightarrow \infty$ and thus cancel out.

B.2 SVGD Kernel

In our experiments, we employ an additive RBF kernel. We also considered a product of RBF kernels, though, found that the additive kernel composition performed better. This additive kernel is defined as

$$k((\mathbf{Z}, \Theta, \Gamma, \Theta_{\mathcal{I}}), (\mathbf{Z}', \Theta', \Gamma', \Theta'_{\mathcal{I}})) := \exp\left(-\frac{\|\mathbf{Z} - \mathbf{Z}'\|^2}{2\tau_Z}\right) + \exp\left(-\frac{\|\Gamma - \Gamma'\|^2}{2\tau_{\Gamma}}\right) + \exp\left(-\frac{\|\Theta - \Theta'\|^2}{2\tau_{\Theta}}\right) + \exp\left(-\frac{\|\Theta_{\mathcal{I}} - \Theta'_{\mathcal{I}}\|^2}{2\tau_{\Theta_{\mathcal{I}}}}\right) \quad (29)$$

with lengthscales $\tau_Z, \tau_{\Gamma}, \tau_{\Theta}$. For brevity, we also write $k(\Psi, \Psi')$ for (29) where $\Psi := (\mathbf{Z}, \Theta, \Gamma, \Theta_{\mathcal{I}})$. For SVGD, the kernel introduces repulsive forces which make the particles disperse well across the domain (see F). Importantly, the lengthscales hyperparameters provide the possibility to fine-tune the repulsion and hence calibrate our inference model. We show this in Sec. E.2.

B.3 Algorithm overview

We provide a pseudocode of our algorithm with its SVGD instantiation in Alg. 1.

C Marginal Inference with the BGe score

In addition to joint posterior inference that includes the *parameters* Θ of the model, we also consider the *marginal* posterior $p(\mathbf{G}|\mathbf{D})$. We employ the commonly used Bayesian Gaussian Equivalent (BGe) marginal likelihood that scores Markov equivalent structures equally [16, 17]. This model factorises the marginal likelihood into components for each node given its parents. Details on the computation of the BGe score are provided by Kuipers et al. [32]. Other good explanations are given by Grzegorzczak [22] and Kuipers and Moffa [31].

Compared to the case of considering parameters Θ , the marginal likelihood does not yield factorization over different datasets. That is,

$$p(\mathbf{D}|\mathbf{G}, \mathcal{I}^{\text{tar}}) \neq \prod_{k=1}^M p(\mathcal{D}_k|\mathbf{G}, \mathcal{I}_k^{\text{tar}})$$

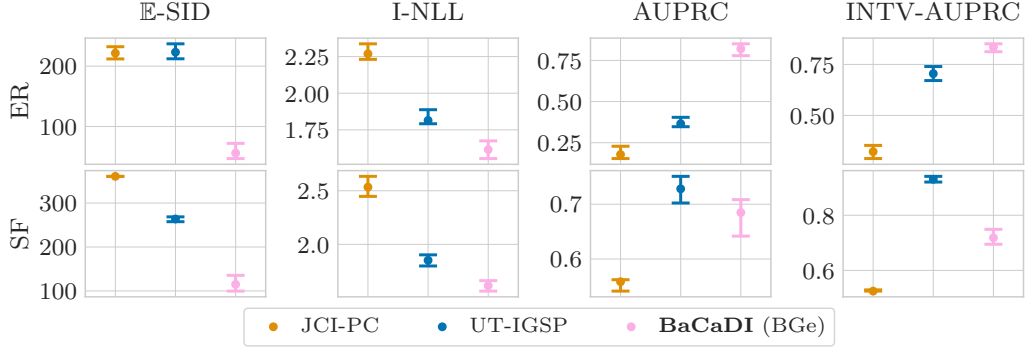


Figure 7: Additional results for Linear Gaussian BNs with $d = 20$ nodes. Here, we use the BGe score [16, 17] that marginalizes out the parameters of a linear Gaussian model. We again see how BaCaDI better predicts causal mechanisms across all settings. Note that DCDI-G is not included since it always performs joint inference with parameters.

Instead, we have to consider the *fused* data from all contexts by

$$\mathbf{X} = \begin{bmatrix} \mathbf{x}_1^T \\ \mathbf{x}_2^T \\ \vdots \\ \mathbf{x}_N^T \end{bmatrix} \in \mathbb{R}^{N \times d} \quad \text{with} \quad \mathbf{c} = \begin{bmatrix} c_1 \\ c_2 \\ \vdots \\ c_N \end{bmatrix} \in \{0, \dots, M\}^N \quad (30)$$

for $N = \sum_{k=1}^M n_k$ and variables $c_i \in \{0, \dots, M\}$ that indicate from which context sample \mathbf{x}_i originates. As before, $c_i = 0$ denotes the observational context.

Interventions. When considering hard interventions, we cut off the connections of a variable to its parents. This effectively means that the data at this variable only contributes a constant (wrt. the current hypothesis graph) factor to the likelihood, and thus the scoring of a hypothesis graph should not be affected. In other words, when computing the score for a certain variable j in the graph \mathbf{G} , we drop all datapoints in \mathbf{X} where j was the target of a hard intervention and then compute the BGe score for the remaining datapoints $\hat{\mathbf{X}}_j$. In our implementation, we achieve this by masking out datapoints in \mathbf{X} . This enables us to still make use of the Gumbel-Softmax estimator for the Bernoulli intervention targets.

Priors. Following the notation of Geiger and Heckerman [17] and Kuipers et al. [32], we use the standard effective sample size hyperparameters $\alpha_\mu = 1$ and $\alpha_\omega = d + 2$. Moreover, we use the diagonal form as the Wishart inverse scale matrix for the Normal-Wishart parameter prior underlying the BGe score (cf. [22]) with a prior mean of $\boldsymbol{\mu} = [0, \dots, 0]^T$.

For interventions, we use the same approach but set the prior values $\boldsymbol{\mu}$ to the real intervention mean from which the interventions were sampled. We then compute a BGe score for the intervened datapoints given an empty graph in order to have comparable likelihood. This helps when estimating the intervention targets that otherwise

Experiments. We evaluate BaCaDI using the marginal BGe score to the baselines of JCI-PC and UT-IGSP. Note that the algorithms of both JCI-PC and UT-IGSP are not affected by the different score; the difference is the scoring of the predicted graph structures, where we compute a likelihood score using the marginal BGe (replacing the MLE parameter estimate). We do not compare to DCDI-G as it always performs joint inference with parameters. Similar to Sec. 7, we focus on linear Gaussian BNs with $d = 20$ nodes. We report the results in Fig. 7. As done previously, we select the models with the lowest heldout I-NLL.

We again see how BaCaDI outperforms related methods in most metrics, particularly \mathbb{E} -SID and I-NLL. Only UT-IGSP performs competitively for AUPRC and INTV-AUPRC of SF graph structures, but fails to be on par with BaCaDI in other settings. These results resonate with the other experimental evaluations, showing promising results for making causal structure predictions.

D Experimental Setup

In the following, we describe the models, datasets and implementations that were used to perform experiments in detail.

D.1 Model Details & BaCaDI

First, we discuss the models of graphs as well as the exact usage of BaCaDI².

Graphs. We consider DAGs that follow either Erdős-Rényi (ER) [19] or scale-free (SF) [4] distributions. ER graphs follow a prior distribution

$$p(\mathbf{G}) \propto q^{\|\mathbf{G}\|_1} (1 - q)^{\binom{d}{2} - \|\mathbf{G}\|_1} \quad (31)$$

that describes that each edge exists independently w.p. q . For SF graphs, we define a prior

$$p(\mathbf{G}) \propto \prod_{i=1}^d (1 + \|\mathbf{G}_i\|_1)^{-3} \quad (32)$$

analogous to their power law degree distribution $p(\text{deg}) \sim \text{deg}^{-3}$. \mathbf{G}_i describes the i -th row of the adjacency matrix. For all our experiments, we use priors that result in $2d$ edges in expectation. Building on Lorch et al. [36], BaCaDI can incorporate such a graph distribution in the prior $p(\mathbf{Z})$ (see Sec. 4.2 in their paper).

Overview: Gaussian BNs. As instantiations of BaCaDI’s inference models that describe the local conditional distributions, we consider Bayesian networks with additive Gaussian noise. This means that the variables $\mathbf{x} = (x_1, \dots, x_d)$ follow a distribution

$$p(x_i | \Theta, \mathbf{G}) = \mathcal{N}(f(x_{\text{pa}_{\mathbf{G}}(i)}), \Theta), \sigma_i) \quad (33)$$

For the inference with BaCaDI, we assume a fixed observation noise $\sigma_i^2 = \sigma^2 = 0.1$.

The function f can be modelled in different ways as follows.

Linear BNs. Linear Gaussian BNs model the mean of a given variable as a linear function of its parents:

$$p(\mathbf{x} | \Theta, \mathbf{G}) = \mathcal{N}((\mathbf{G} \circ \Theta)^T \mathbf{x}, \sigma \mathbf{I}), \quad (34)$$

where \circ denotes the element-wise multiplication. We use this parametrization as it allows for constant dimensionality of $\Theta \in \mathbb{R}^{d \times d}$ and the elementwise multiplication only keeps the parents of each variable. Moreover, this allows the use of the Gumbel-Softmax estimator in Eq. 14.

As a prior, we use a standard Gaussian $p(\Theta_{i,j} | \mathbf{G}_{i,j} = 1) = \mathcal{N}(0, 1)$.

Nonlinear BNs. The local conditionals can be extended to *nonlinear* dependencies modelled by neural networks. We consider feed-forward neural networks of the form

$$\text{FFN}(\mathbf{x}; \Theta) := \Theta^{(L)} \sigma(\dots, \Theta^{(1)} \mathbf{x} + \theta_b^{(1)}) \dots + \theta_b^{(L)}, \quad (35)$$

where $\Theta = ((\Theta^{(L)}, \theta_b^{(L)}), \dots, (\Theta^{(1)}, \theta_b^{(1)}))$ describe the parameters of the l -th layer for $l \in \{1, \dots, L\}$. The function σ is the element-wise nonlinear activation function and $\theta_b^{(l)}$ is the bias. This then gives the distribution

$$p(\mathbf{x} | \Theta, \mathbf{G}) = \prod_{i=1}^d \mathcal{N}(x_i; \text{FFN}(\mathbf{G}_i^T \circ \mathbf{x}; \Theta_i), \sigma). \quad (36)$$

Note that we thus have one neural network defined by Θ_i for each of the local conditional distributions of variable i , that is, d networks in total. For all experiments, we use one hidden layer with 5 units and the sigmoid activation function.

As a prior for the parameters, we analogously use a standard Gaussian with mean 0 and variance 1.

Interventions. We model interventions using a Gaussian likelihood $p_i^{I_k}(x_i | \Theta_{I_k}) = \mathcal{N}(x_i | \mu_{k,i}^I, \sigma_I)$ with fixed variance $\sigma_I^2 = 0.5$. We infer the means $\Theta_{I_k} = [\mu_{k,1}^I, \dots, \mu_{k,d}^I]$ for which we set a wide

²Some parts of the model descriptions follow the appendix in [36] and are included for completeness.

Gaussian prior $p(\Theta_{I_k} | I_k^{\text{tar}}) = \prod_{i \in I_k^{\text{tar}}} p(\mu_{k,i}^I | I_{k,i}^{\text{tar}} = 1) = \prod_{i \in I_k^{\text{tar}}} \mathcal{N}(\mu_{k,i}^I | 0, 10)$. This reflects an uninformative prior over a large effect range of the interventions.

Initialization. For the linear Gaussians, the parameters are initialized closed to zero via $\Theta_{\text{init}} \sim \mathcal{N}(0, \sigma_{\text{init}} \mathbf{I})$ with $\sigma_{\text{init}} = 0.3$. The closeness to zero is important to avoid inducing a bias at the start of the SVGD inference process. Similarly, we sample $\Theta_{\mathcal{L}, \text{init}} \sim \mathcal{N}(0, \sigma_{\mathcal{L}, \text{init}} \mathbf{I})$ with $\sigma_{\mathcal{L}, \text{init}}^2 = 0.1$.

For nonlinear Gaussians, we use the Glorot (sometimes called Xavier) normal to initialize the weights of the neural networks. [20].

D.2 Data Generation for the Synthetic Causal Inference Tasks

The data generation is done as follows: we first sample a random graph (either ER or SF) and then sample random parameters. We collect data samples by iterating through the topological ordering of the graph and sample a variable given its local parents. Since we consider additive Gaussian models, each variable is described by a distribution of the form $x_i | \Theta, \mathbf{G} \sim \mathcal{N}(f(x_{\text{pa}_{\mathbf{G}}(i)}), \Theta), \sigma_i)$ where f is either a linear function or a nonlinear feedforward neural network (cf. Sec. D.1). The noise variables σ_i are sampled per variable and fixed once from $\sigma_i^2 \sim \mathcal{U}[0.05, 0.15]$. If the noise variables had the same variance across all variables in the graph, this would render identification possible [48].

Parameters. The parameters and generative models are initialized as follows:

- *Linear BNs:* We sample the parameters Θ uniformly and independently from $\mathcal{U}([-2, -0.5] \cup [0.5, 2])$ in order to bound the weights sufficiently away from zero.
- *Nonlinear BNs:* The NNs for each local conditional are the same model as used for BaCaDI as well as DCDI-G, that is, a fully connected NN with single hidden layer of size of 5 with biases. The nonlinear activations are sigmoid functions. All weights and biases are drawn randomly and independently from a Gaussian $\mathcal{N}(0, 1)$.

Interventions. As described in the main text, we perform *hard* interventions on every node for the 20-node graphs. We create random values by first sampling $\hat{\mu}_{k,i} \sim \mathcal{N}(0, 2)$ and then setting $\mu_{k,i}^I = \text{sign}(\hat{\mu}_{k,i}) \cdot 5 + \hat{\mu}_{k,i}$. This ensures that the interventions performed are bounded away from zero and out-of-distribution. If a variable x_i is the target of the intervention in context k , we then have $p_i^{I_k}(x_i | \Theta_{I_k}) = p_i^{I_k}(x_i | \mu_{k,i}^I) = \mathcal{N}(x_i; \mu_{k,i}^I, \sigma_I)$, where $\sigma_I^2 = 0.5$.

D.3 Data generation with the SERGIO gene-expression simulator

SERGIO [10] is a single-cell expression simulator for gene regulatory networks (GRNs). The software tool can generate realistic single-cell transcriptomics datasets based on a user-defined graph input that describes the regulatory network. SERGIO uses stochastic differential equations to simulate a gene’s expression dynamics as a function of the changing levels of its regulators. The simulations resemble the data collected by modern high-throughput, single-cell RNA sequencing (scRNA-seq) technologies and are thus more practically-relevant than simulators approximating “bulk” microarray data [52]. For more details, we refer to the original paper by Dibaenia and Sinha [10]. In the following, we give a brief overview of how we simulate scRNA-seq data with SERGIO. For this, we use an implementation that is adapted from the open-source code available under <https://github.com/PayamDiba/SERGIO>, which is published under a GPL-3.0 license.

Simulation. SERGIO generates synthetic scRNA-seq data \mathbf{D} for a given causal graph with d genes by first simulating clean gene expression data and then corrupting these expressions with technical measurement noise. The N observations in \mathbf{D} correspond to N cell samples, i.e. one row in \mathbf{D} describes the joint expression of the d genes in a single cell. For simplicity, we do not add the technical noise modules in our experiments.

To simulate the single-cell gene expressions, SERGIO samples randomly-timed expression snapshots from the steady state of the stochastic dynamical system modeling the GRN. In this regulatory process, the genes are expressed at rates influenced by other genes using the chemical Langevin equation. The source nodes in the causal graph \mathbf{G} are denoted master regulators (MRs), whose expressions evolve at constant production and decay rates. The downstream gene expressions evolve non-linearly under production rates caused by the expression of their causal parents in \mathbf{G} . To model different cell types, SERGIO varies the specifications of the MR production rates, which significantly influence the

evolution of the system. As a result, the data contains variation across cell types and due to biological noise within cells of the same type. In our experiments, we generate single-cell samples collected from ten cell types [10].

Interventions. We consider *knockout interventions* that clip the expression of a specific gene to zero. To this end, we extend SERGIO by forcing the production rate of knocked-out genes to be zero during simulation. As described in the main text, we do this for $M = 10$ gene targets and arrive at 11 contexts, including the observational setting.

Parameters. To specify the simulation parameters of SERGIO, we follow the settings suggested by Dibaeinia and Sinha [10] for synthetic data generation. Given a causal graph \mathbf{G} , the simulation for c cell types of d genes is governed by the following parameters:

- $k \in \mathbb{R}^{d \times d}$, $k_{i,j} \sim \mathcal{U}[1, 5]$: interaction strength if edge $i \rightarrow j$ exists in \mathbf{G}
- $b \in \mathbb{R}_+^{d \times c}$, $b_{i,j} \sim \mathcal{U}[1, 3]$: MR production rates if j is a source node in \mathbf{G}
- $\gamma \in \mathbb{R}_+^{d \times d}$, $\gamma_{i,j} = 2$: Hill function coefficients controlling nonlinearity of interactions
- $\lambda \in \mathbb{R}^d$, $\lambda_i = 0.8$: decay rates per gene
- $\zeta \in \mathbb{R}_+^d$, $\zeta_i = 1.0$: scale of stochastic process noise in chemical Langevin equation

We standardize the data for all methods by subtracting the empirical mean and dividing by the standard deviation.

D.4 Baselines & Implementation

In this section, we provide additional details on the baseline methods and their implementations used in our experiments. Our source-code and instructions on how to reproduce results are available under <https://www.dropbox.com/sh/5vtj4zp9h8sr9zq/AACkJ5naAxxXnpIByNEezI4Ia?dl=0>.

For all methods, we use implementations adapted from the source code of DCDI available under <https://github.com/slachapelle/dcdi> (where the authors also included their baselines' code). The implementation of JCI-PC is a modified version of the R package using code from the JCI repository <https://github.com/caus-am/jci/tree/master/jci>. UT-IGSP has an implementation available from <https://github.com/uhlerlab/causaldag>.

DAG Bootstrap. To compare all methods in Bayesian model averaging, we employ the nonparametric DAG bootstrap [15]. It performs model averaging by bootstrapping the observations \mathbf{D} to yield a collection of synthetic data sets, each of which is used to learn a single graph. We sample with replacement from \mathbf{D} for each dataset \mathcal{D}_k individually. The collection of unique single graphs approximates the posterior by weighting each graph by its unnormalized posterior probability.

All of the methods are evaluated with 20 bootstrap samples, i.e. the same number of samples as particles used for the SVGD instantiation of BaCaDI. For DCDI-G, we only use 5 bootstrap samples due to the significantly longer runtimes.

JCI-PC. The Joint Causal Inference (JCI) framework [43] introduces a general formulation to extend the initial causal graph by auxiliary nodes that describe the different contexts, effectively performing causal discovery over a graph of size $d + M$. This approach can be instantiated with different standard algorithms. In our experiments, we use the PC algorithm [56], which relies on conditional independence tests (CI) to discover the Markov Equivalence Class (MEC), i.e. the skeleton of a graph with v-structures as well as possible identifiable edge directions. The PC algorithm uses a Gaussian CI test with significance threshold α^{JCI} , which are best-suited for Gaussian BNs.

For computing the graph metrics, we compute the \mathbb{E} -SID between the CPDAGs of the GT graph and predictions of JCI-PC. Additionally, we favor JCI-PC when computing AUPRC scores. See Sec. D.5 for more details.

To arrive at a DAG that we can use to estimate MLE parameters and compute log-likelihood metrics, we generate a random consistent expansion of the CPDAG as defined by Chickering [8] using the algorithm by Dor and Tarsi [11]. That is, we generate a DAG s.t. the CPDAG has the same skeleton and v-structures and every directed edge in the CPDAG has the same direction in the DAG.

UT-IGSP. The interventional greedy sparsest permutation (IGSP) method [60, 62] proposes an algorithm that learns causal structures via local scores based on CI relations and permutation search. The work is extended by Squires et al. [57] to the case of unknown targets (UT-IGSP). Analogous to JCI-PC, IGSP uses Gaussian CI and invariance tests with parameters $\alpha^{\text{UT-IGSP}}$ and $\alpha_{\text{inv}}^{\text{UT-IGSP}}$. Since we study the low sample setting, it is possible that the algorithm as provided by their open source implementation fails to compute an essential correlation matrix. Specifically, the algorithm computes a correlation matrix that becomes singular in the case when the number of unique samples is smaller than the number of variables considered, thus rendering an inversion of this matrix impossible. In case this happens, we retry the inference with a halved $\alpha^{\text{UT-IGSP}}$ confidence threshold. The maximum number of restarts is set to 10, and the bootstrap sample is dropped in case this maximum is reached.

Similar to JCI-PC, the \mathbb{E} -SID is computed as the midpoint of the lower and upper bound between the CPDAGs of the GT graph and predictions of UT-IGSP. As for JCI-PC, we favor UT-IGSP when computing AUPRC scores. See Sec. D.5 for more details. Likewise, we obtain a DAG by generating a random consistent expansion of the CPDAG to compute the log-likelihood metrics.

DCDI-G. Brouillard et al. [6] introduced Differentiable Causal Discovery from Interventional Data (DCDI), which performs causal structure learning via the augmented Lagrangian method. The algorithm formulates a continuous-constrained optimization problem that relies on stochastic gradient descent and neural networks to fit the local conditionals.

To ensure a fair comparison, we employ the exact same likelihood model as used for the nonlinear Gaussian BNs used in BaCaDI, that is, a feedforward neural network with one hidden layer of size 5 and Gaussian additive noise. This model is called DCDI-G in [6]. However, we use a smaller neural network to model the means of the local conditional distributions than originally used by Brouillard et al. [6]. In initial experiments with DCDI-G, we observed strong overfitting due to our low-sample regime and thus reduced the model capacity. As suggested by Brouillard et al. [6], we use the leaky ReLU with negative slope of 0.25 as elementwise activation function. To obtain comparable log-likelihood metrics, we fix the noise variables to $\sigma^2 = 0.1$ as done for BaCaDI. These noise variables could generally be learned by both methods.

D.5 Metrics

Our reported metrics focus on three essential aspects of our inference problem: causal graph prediction, intervention detection, and learning the local conditional distributions of the individual variables.

- *SID*: The *Structural Interventional Distance* (SID) [49] quantifies the closeness between two DAGs in terms of how well their interventional adjustment sets coincide. Since we perform posterior inference and arrive at a distribution over graphs, we consider the *expected* SID, which is defined as

$$\mathbb{E}\text{-SID}(p, \mathbf{G}_{\text{gt}}) := \sum_{\mathbf{G}} p(\mathbf{G}|\mathcal{D}) \cdot \text{SID}(\mathbf{G}, \mathbf{G}_{\text{gt}}) \quad (37)$$

To compute the SID, we use the implementation provided by the Causal Discovery Toolbox [29]. Since UT-IGSP and JCI-PC only return a CPDAG of the Interventional Markov Equivalence Class (I-MEC), we calculate the lower and upper bound of the SIDs in the I-MEC and report their midpoint as the \mathbb{E} -SID. The DAG bootstrap variants for all baselines as well as BaCaDI use the weighted mixture rather than the empirical distribution of samples. The weight is based on the unnormalized log-likelihood achieved on the bootstrap sample.

- *SHD*: The structural hamming distance (SHD) reflects the graph edit distance to the ground truth DAG. However, it often does not properly reflect the closeness of two DAGs in terms of their causal interpretation. For instance, the trivial prediction of the empty graph achieves competitive SHD scores for the sparse graphs we consider in this paper. In our main text, we thus focus on the \mathbb{E} -SID as well as other metrics that together better assess the quality of causal graph predictions. For completeness, we report the \mathbb{E} -SHD results in Appx. E.5.
- *Threshold metrics*: Treating the edge prediction as a classification task, we compute the area under the precision recall curve (AUPRC) for pairwise edge prediction based on the posterior marginals $p(g_{ij} = 1|\mathbf{D})$. This marginal is defined as the posterior mean of an indicator variable for the presence of the edge: $p(g_{ij} = 1|\mathbf{D}) = \mathbb{E}_{p(\mathbf{G}|\mathbf{D})} \mathbf{1}[g_{ij} = 1]$. The AUPRC provides more insight into

predictive performance than, e.g., the AUROC because sparse graphs translate to highly imbalanced edge classification tasks.

For JCI-PC and UT-IGSP, which both return a CPDAG with edges that are undecided, we favor the methods when computing the AUPRC metric. Specifically, we orient a predicted undirected edge correctly when a ground truth edge exists and only count a falsely predicted undirected edge as a single mistake.

- *Interventional AUPRC*: Similarly, we report the *interventional* AUPRC (INTV-AUPRC) for the classification of intervention targets. The INTV-AUPRC captures how well an algorithm predicts which variables have been intervened on. Since we assume sparse interventions, this metric better captures a model’s performance for the imbalanced classification task.
- *I-NLL*: We compute the average negative *interventional log-likelihood* (I-LL) on $M^{\text{test}} = 10$ held-out interventional datasets $\mathbf{D}^{\text{test}} = \{\mathcal{D}_1^{\text{test}}, \dots, \mathcal{D}_{10}^{\text{test}}\}$, where different interventions are performed compared to the training datasets. Each interventional test dataset comprises 100 samples and has known intervention targets $I_{\text{test},k}^{\text{tar}}$ and effect distributions $p(x_i | \Theta_{I_{\text{test},k}})$

The I-NLL is computed via

$$\text{I-NLL}(p, \mathbf{D}^{\text{test}}) := -\frac{1}{M^{\text{test}}} \sum_{k=1}^{M^{\text{test}}} \mathbb{E}_{p(\mathbf{G}, \Theta | \mathbf{D})} \left[\frac{1}{|\mathcal{D}_k^{\text{test}}|} \log p(\mathcal{D}_k^{\text{test}} | \mathbf{G}, \Theta, I_{\text{test},k}^{\text{tar}}, \Theta_{I_{\text{test},k}}) \right].$$

Since UT-IGSP and JCI-PC are not equipped with local conditional distributions, we use the linear Gaussian maximum-likelihood parameters (MLE), which can be computed in closed-form [24]. For the nonlinear datasets, this creates a model mismatch since the closed form is only available for linear Gaussian BNs.

D.6 Hyperparameter Search

To ensure a fair comparison, we perform a hyperparameter search for all baselines. The search ranges can be found in Table 1. Throughout all experiments, we use at least 20 hyperparameter samples and aggregate results over 30 different random seeds and graphs.

Method	Hyperparameter	Comment	Search range
BaCaDI	α	Linear slope temperature for Bernoulli	$\mathcal{U}[1, 3]$
	β	Linear slope temperature for acyclicity prior	$\log_{10} \mathcal{U}[-3, -1]$
	τ_Z	Kernel lengthscale	$\log_{10} \mathcal{U}[-1, 1.7]$
	τ_γ	Kernel lengthscale	$\log_{10} \mathcal{U}[-1, 1.7]$
	τ_θ	Kernel lengthscale	$\log_{10} \mathcal{U}[1.2, 5]$
	λ	Intervention sparsity prior	$\log_{10} \mathcal{U}[-1, 2]$
JCI-PC	α^{JCI}	CI tests	$\log_{10} \mathcal{U}[-5, -1]$
UT-IGSP	$\alpha^{\text{UT-IGSP}}$	CI tests	$\log_{10} \mathcal{U}[-5, -1]$
	$\alpha_{\text{inv}}^{\text{UT-IGSP}}$	Invariance tests	$\log_{10} \mathcal{U}[-5, -1]$
DCDI-G	batch size	-	$\mathcal{U}(\{16, 32, 64\})$
	λ_R	Sparsity coefficient for interventions	$\log_{10} \mathcal{U}[-8, -1]$
	λ	Sparsity coefficient for graph	$\log_{10} \mathcal{U}[-3, -1]$
	h	Convergence threshold	$\log_{10} \mathcal{U}[-8, -6]$

Table 1: Hyperparameter search space for all methods

E Additional Experiments

E.1 Larger datasets

We report additional results when doubling the dataset size, i.e. we collect $n_0 = 200$ observational samples and $n_k = 20$ samples per interventional context. The results for synthetic linear and nonlinear Gaussian BNs can be found in Fig. 8 and Fig. 9, respectively.

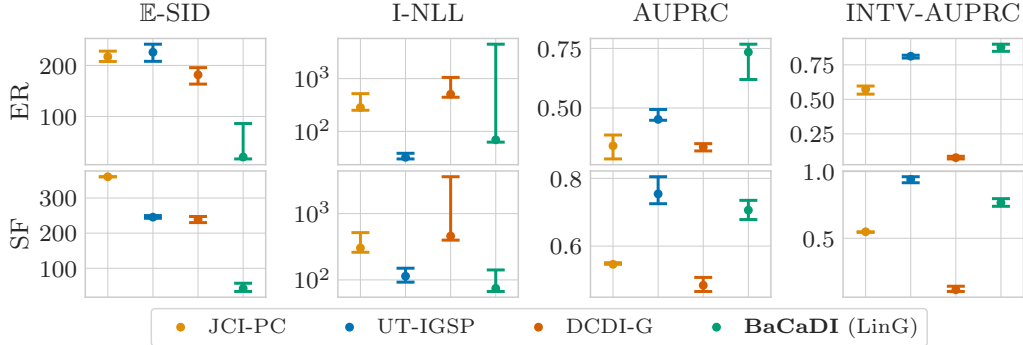


Figure 8: **Linear Gaussian with more data.** Joint posterior inference over CBNs and interventions for *linear Gaussian* ground-truth CBNs. The results are for data from ER-2 (top) and SF-2 (bottom) graphs with $d = 20$ variables and $M = 20$ contexts. Here, we double the dataset size to $N = 600$ samples in total. Similar to the previous setting with lower sample sizes, BaCaDI is consistently the most competitive method.

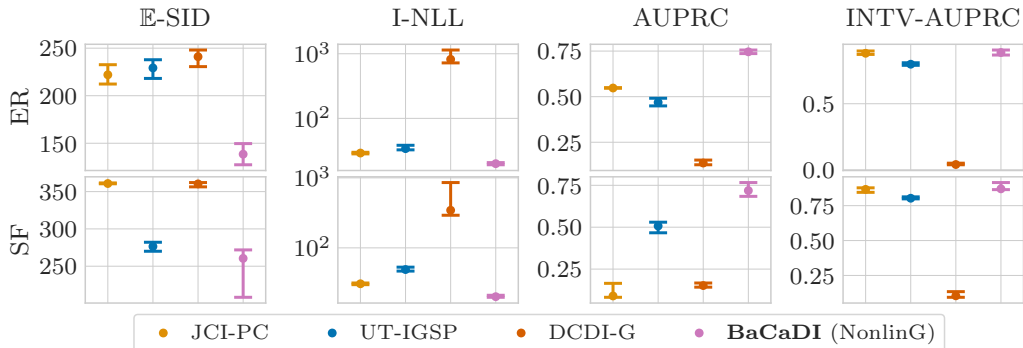


Figure 9: **Nonlinear Gaussian with more data.** Joint posterior inference over CBNs and interventions for *nonlinear Gaussian* ground-truth CBNs. The results are for data from ER-2 (top) and SF-2 (bottom) graphs with $d = 20$ variables and $M = 20$ contexts. Here, we double the dataset size to $N = 600$ samples in total. BaCaDI performs the best across all metrics.

E.2 Calibration

Having compared BaCaDI with the baselines across the metrics for causal structure learning, we provide additional experiments to show how BaCaDI captures *epistemic uncertainty*. We again utilize the concept of calibration [21, 33] to quantify the reliability of our uncertainty estimates. First, we give the calibration plots for the synthetic datasets used in the main text. Then, we give an ablation study illustrating how BaCaDI offers the ability to fine-tune its calibration through the kernel parameters of SVGD.

Calibration for synthetic datasets. We show the calibration for all methods with the synthetic datasets used in the main text. The calibration plots can be found in Fig. 10. Notably, BaCaDI is the only method that does not give grossly overconfident predictions. Instead, it is conservative in predicting edges for the linear BNs, and gets closest to the ideal calibration line for nonlinear BNs.

Ablation study. In addition to the ability of inferring the causal structure and mechanisms, we now demonstrate the flexibility of calibrating the inference behavior of BaCaDI. Through the use of SVGD and a kernel that can be designed specifically for the application, BaCaDI can be fine-tuned to a desired calibration, i.e., degrees of confidence in its posterior estimate. We show different inference results in Fig. 11 for linear as well as nonlinear datasets. Depending on the length scale hyperparameters for the kernel in 29, we see that the predictions of BaCaDI can be easily adapted to varying levels of confidence. Our method thus enables us to flexibly model the epistemic uncertainty when dealing with limited data.

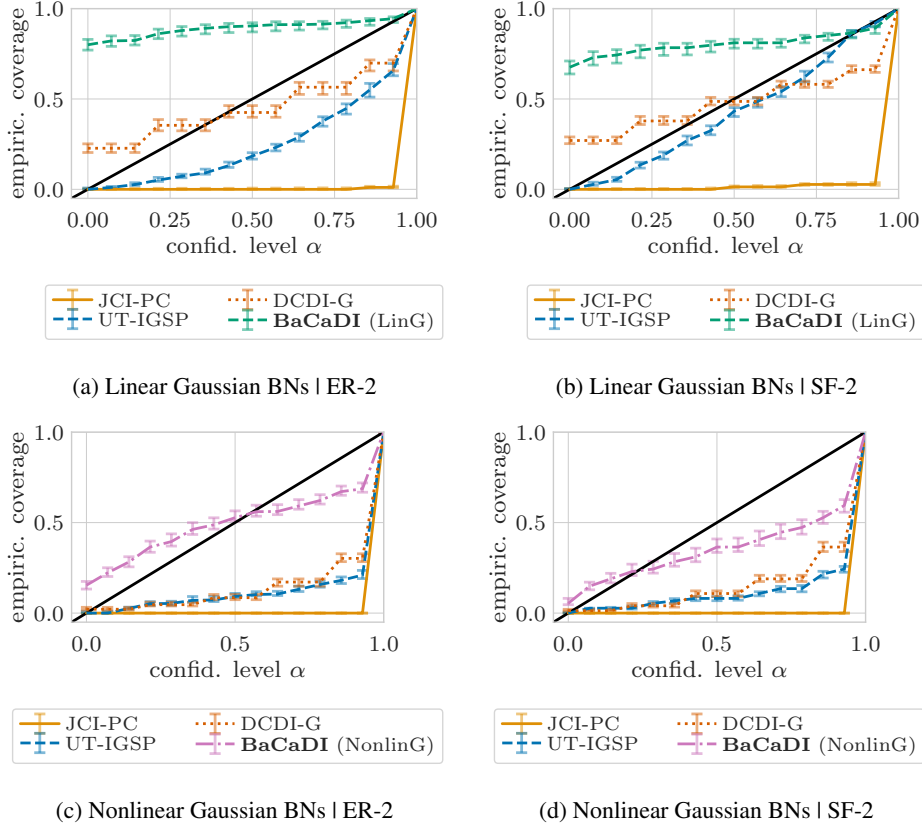


Figure 10: **Calibration plots for the synthetic datasets.** The top row shows the calibration plots for linear Gaussian BNs for ER graphs (left) and SF graphs (right). The bottom row shows the nonlinear Gaussian BNs. All results correspond to the same models and configuration as the results reported in the main text. Notably, BaCaDI is the closest to the ideal calibration line for nonlinear BNs and does not deliver overconfident predictions for linear BNs.

E.3 Observational vs. Interventional Data

As an additional interesting use case, we evaluate how interventional data helps predicting the causal structure with BaCaDI. In general, intervening on variables in the system and observing the outcome provides information that helps discovering the causal mechanisms. In the perfect setting, when the intervention targets are fully known, they increase identifiability by shrinking the interventional Markov equivalence class [23]. However, the information gain can be limited when the intervention targets are unknown [57].

We investigate how BaCaDI can leverage such unknown interventions compared to using just observational data. To that end, we evaluate 3 different settings: i) when only observational data is available, ii) interventional data with full knowledge of the interventions, and iii) unknown interventions. When the interventions are known, the posterior inference of BaCaDI can be reduced to Eq. 5.

We consider nonlinear Gaussian BNs for $d = 20$ node graphs. All methods receive the exact same number of samples for inference. That is, we collect $n_0 = 300$ samples from the ground-truth BN without interventions for the observational dataset. As before, the interventional datasets have $n_0 = 100$ observations and $n_k = 10$ samples per interventional context. We report the results in Fig. 12.

We observe that BaCaDI achieves significantly better results when interventional data is available. The case of known interventions serves as a natural baseline, where BaCaDI achieves the best performance and gets closest in recovering the true causal structure. This is most clearly shown by the E-SID and AUPRC scores. Notably, BaCaDI is able to get close this baseline even when interventions are unknown and outperforms the setting where just observational data is available.

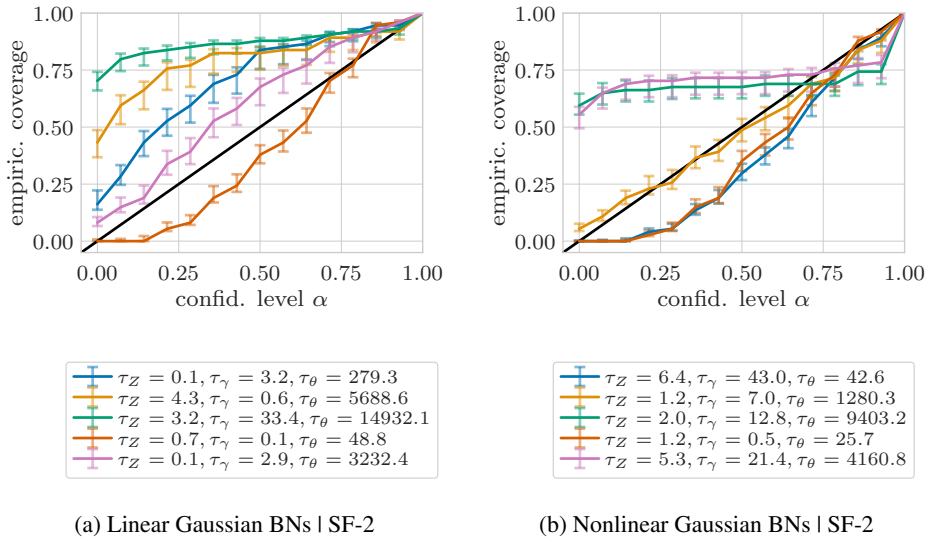


Figure 11: **Calibration plot sweeps.** We show calibration plots for varying kernel lengthscales for $d = 20$ node SF graphs for linear Gaussian BNs (left) and nonlinear Gaussian BNs (right). BaCaDI offers the possibility to fine-tune the calibration of the predictive model depending on the application and desired results. It thus can properly take into account the *epistemic uncertainty* when dealing with limited data.

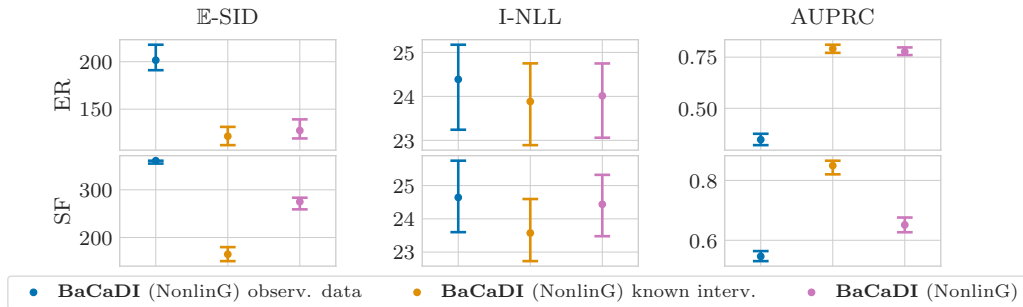


Figure 12: **Comparison: Observational data vs. known and unknown interventions.** Additional results comparing BaCaDI with observational data against known and unknown interventions for nonlinear Gaussian BNs for $d = 20$ node graphs. As a natural baseline, the setting of knowing the intervention targets and effects leads to the best performance across all metrics. When the interventions are unknown, BaCaDI achieves results close to this baseline. Notably, it outperforms the setting where just observational data is available.

This shows the benefit of performing and collecting interventions even when some of the effects may be unknown and is a promising result for future work.

E.4 50 node graphs

As additional experiments, we perform posterior inference for larger graphs with 50 nodes in total. Analogous to the previous evaluations, we consider synthetic linear Gaussian BNs with hard interventions on every node. We use a larger dataset of $n_0 = 200$ observational samples and $n_k = 20$ samples per interventional context. The results are given in Fig. 13. We find that BaCaDI scales to larger graphs and performs competitively across all metrics. In particular, our method outperforms the baselines by a large margin in terms of the \mathbb{E} -SID and AUPRC for ER graphs.

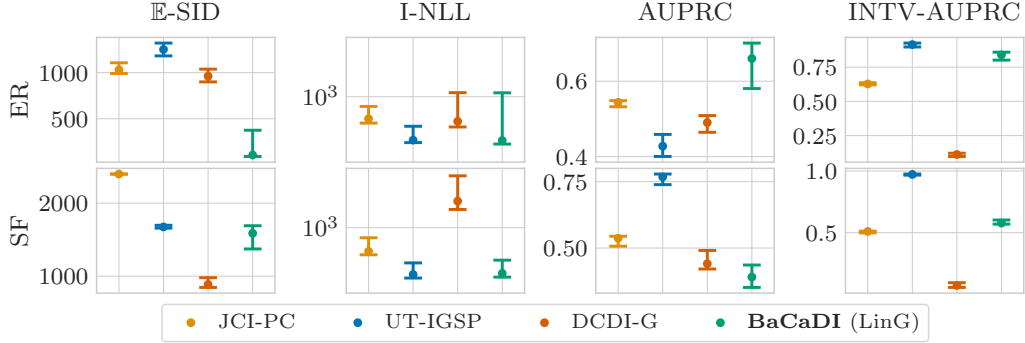


Figure 13: **Linear Gaussian BNs with 50 nodes.** Additional results comparing BaCaDI on larger graphs with $d = 50$ nodes for Linear Gaussian BNs for ER-2 (top) and SF-2 (bottom). BaCaDI performs competitively across all metrics. In particular, it makes significantly better causal mechanism predictions for ER graph as captured by the \mathbb{E} -SID.

E.5 Structural Hamming Distance

For completeness, we include the *Expected Structural Hamming Distance* (\mathbb{E} -SHD) metric for all results discussed in the main text for $d = 20$ node graphs in Table 2. Analogous to the \mathbb{E} -SID, the \mathbb{E} -SHD is defined as $\mathbb{E}\text{-SHD}(p, \mathbf{G}_{\text{gt}}) := \sum_{\mathbf{G}} p(\mathbf{G}|\mathcal{D}) \cdot \text{SHD}(\mathbf{G}, \mathbf{G}_{\text{gt}})$. The SHD reflects the graph edit distance where wrongly inverted edges are counted as only one error. However, while it captures closeness to the ground truth graph, trivial predictions like the empty graph achieve competitive results for sparse graphs. For example, in the setting of $d = 20$ nodes and $2d$ edges in expectation, the empty graph will achieve a \mathbb{E} -SHD of 40 in expectation. Similar conclusions hold if only very few edges are predicted. In the main text, we thus resort to the \mathbb{E} -SID as well as additional metrics that together report an accurate description of the quality of inference.

	JCI-PC	UT-IGSP	DCDI-G	BaCaDI (LinG)	BaCaDI (NonlinG)
Linear Gaussian BNs graphs:					
ER	38.97 (1.65)	41.38 (2.53)	63.29 (4.52)	50.32 (10.98)	-
SF-2	37.42 (0.32)	34.35 (1.18)	51.68 (3.67)	36.48 (6.12)	-
Nonlinear Gaussian BNs graphs:					
ER	38.93 (1.65)	35.09 (1.76)	64.91 (2.61)	-	18.73 (1.85)
SF-2	37.00 (0.00)	33.75 (0.48)	57.92 (2.69)	-	23.55 (1.43)
SERGIO graphs					
SF-2	44.29 (0.70)	45.05 (1.88)	56.39 (1.63)	108.71 (3.75)	115.04 (6.22)

Table 2: **Expected Structural Hamming Distance.** We report the \mathbb{E} -SHD for all methods for the main results with $d = 20$ node graphs. We aggregate results over 30 different seeds and report the mean and standard error. While the \mathbb{E} -SHD is a simple and commonly used metric, it can be misleading. For sparse graphs, the trivial prediction of the empty graph achieves competitive \mathbb{E} -SHD scores; similar assessments can be made for predictions with only a few edges. We include the results for completeness.

E.6 Runtimes

We report the average runtimes (in minutes) for all methods and main results for $d = 20$ node graphs in Table 3.

	JCI-PC	UT-IGSP	DCDI-G	BaCaDI (LinG)	BaCaDI (NonlinG)
Linear Gaussian BNs graphs:					
ER	2.07± 0.16	1.31± 0.22	260.03±56.11	51.68±13.12	-
SF-2	2.17± 0.15	1.46± 0.09	176.89±30.46	60.57±22.95	-
Nonlinear Gaussian BNs graphs:					
ER	1.89± 0.07	1.16± 0.06	143.88±12.53	-	491.26±91.74
SF-2	1.92± 0.06	1.41± 0.06	145.43±25.83	-	519.79±97.95
SERGIO graphs					
SF-2	2.36± 0.09	0.42± 0.20	128.04± 9.97	45.11± 1.52	323.11±101.15

Table 3: **Average runtimes** for all methods for the main results with $d = 20$ node graphs. We aggregate results over 30 different seeds and report the mean and standard deviation. All numbers given are in minutes.

E.7 Computational Resources

All experiments reported in this paper were performed in bulk and in parallel on 2-core CPU nodes of an internal cluster. No GPUs were used. We estimate the total compute to amount to roughly 40,000 hours of CPU time.

F Stein Variational Gradient Descent

We here give an overview of Stein Variational Gradient Descent (SVGD) introduced by Liu and Wang [35]. Fundamentally, the work of Liu and Wang [35] connects the mathematical notions of probability discrepancies with a variational inference method, which closely resembles the gradient descent algorithm. For details, we refer to the original paper.

Stein’s identity and discrepancy Formally, let $p(\mathbf{x})$ be a continuously differentiable (i.e. smooth) density supported on $\mathcal{X} \subseteq \mathbb{R}^d$. For a smooth vector function $\phi(\mathbf{x})$, *Stein’s identity* states that for sufficiently regular ϕ , we have

$$\mathbb{E}_{\mathbf{x} \sim p}[\mathcal{A}_p \phi(\mathbf{x})] = 0, \text{ where } \mathcal{A}_p \phi(\mathbf{x}) = \phi(\mathbf{x}) \nabla_{\mathbf{x}} \log p(\mathbf{x})^T + \nabla_{\mathbf{x}} \phi(\mathbf{x}) \quad (38)$$

where \mathcal{A}_p is the Stein operator acting on the function ϕ . This equation can be subsequently used as a discrepancy measure: when considering the expectation over a smooth density q different than p , we obtain the so called *Stein discrepancy* by considering the *maximum violation of Stein’s identity*. That is, we have

$$\mathbb{S}(q, p) = \max_{\phi \in \mathcal{F}} [\mathbb{E}_{\mathbf{x} \sim q} [\text{trace}(\mathcal{A}_p \phi(\mathbf{x}))]^2] \quad (39)$$

for a choice of a set of functions \mathcal{F} , for instance the reproducing kernel Hilbert space (RKHS) denoted by \mathcal{H}^d .

Variational Inference using smooth transforms The goal of variational inference is to approximate a target distribution p using a simpler distribution q^* which minimizes the KL-divergence

$$q^* = \arg \min_{q \in \mathcal{Q}} KL(q||p) \quad (40)$$

In order to minimize the KL-divergence, the authors in [35] consider incremental transforms formed by a small perturbation to the identity map that make up the set of distributions \mathcal{Q} . That is, the transform $\mathbf{T} : \mathcal{X} \rightarrow \mathcal{X}$ is defined as

$$\mathbf{T}(\mathbf{x}) = \mathbf{x} + \epsilon \phi(\mathbf{x}) \quad (41)$$

where ϕ is a smooth function that characterizes the perturbation direction. As a key result, Liu and Wang [35] connect these transforms to the Stein operator and the derivative of the KL divergence. The authors show that if the function ϕ lies in the ball of the vector valued RKHS \mathcal{H}^d , the direction of the steepest descent on the KL divergence between a fixed q and the target p is given by

$$\phi_{q,p}^* = \mathbb{E}_{\mathbf{x} \sim q} [k(\mathbf{x}, \cdot) \nabla_{\mathbf{x}} \log p(\mathbf{x}) + \nabla_{\mathbf{x}} k(\mathbf{x}, \cdot)] \quad (42)$$

where one can easily identify the form of the Stein operator. What is more, the value of the obtained gradient equals the (negative) kernelized Stein discrepancy measure $-\mathbb{S}(q, p)$.

General Algorithm This mathematical result suggests an iterative method that transforms an initial reference distribution q_0 to the target distribution p . Starting with a finite set of random particles $\{\mathbf{x}^{(m)}\}_{m=1}^M$, for some iteration t each particle is updated deterministically according to

$$\mathbf{x}_{t+1}^{(m)} \leftarrow \mathbf{x}_t^{(m)} + \epsilon_t \phi(\mathbf{x}_{t+1}^{(m)}) \quad (43)$$

$$\text{where } \phi(\mathbf{x}) = \frac{1}{M} \sum_{l=1}^M k(\mathbf{x}_{t+1}^{(l)}, \mathbf{x}) \nabla_{\mathbf{x}} \log p(\mathbf{x}) + \nabla_{\mathbf{x}} k(\mathbf{x}_{t+1}^{(l)}, \mathbf{x}) \quad (44)$$

These steps iteratively decrease the KL divergence between q_t and p , ultimately converging.

Importantly, the advantage of SVGD is that it only depends on the gradient of the kernel $k(x, \cdot)$ that can be defined for the application, as well as the score function $\nabla_{\mathbf{x}} \log p(x)$ which can be computed without knowing the (intractable) normalization constant of p . On an intuitive level, the first part of the perturbation direction expression drives the particles to high density regions close to the mode of the target distribution p , whereas the term $\nabla_{\mathbf{x}} k(\mathbf{x}, \cdot)$ acts as a repulsive force that prevents the particles from collapsing together.